NASA TECHNICAL NOTE

NASA TN D-4808

$C.i$

A METHOD FOR COMPUTING LUMINOUS EFFICIENCIES FROM METEOR DATA

by Barrett S. Baldwin, Jr., and H. Julian Allen

Ames Research Center
Moffett Field, Calif.

NASA TN D-4808

A METHOD FOR COMPUTING LUMINOUS EFFICIENCIES

FROM METEOR DATA

By Barrett S. Baldwin, Jr., and H. Julian Allen

Ames Research Center
Moffett Field, Calif.

NATIONAL AERONAUTICS AND SPACE ADMINISTRATION

TABLE OF CONTENTS

A METHOD FOR COMPUTING LUMINOUS EFFICIENCIES

FROM METEOR DATA

By Barrett S. Baldwin, Jr., and H. Julian Allen

Ames Research Center

SUMMARY

The details of a model for the ablation of a stone meteoroid passing through the atmosphere are presented. The model allows for a decrease in mean density due to frothing, which results from the intense heating at low atmospheric pressures. The model is applied to an analysis of meteor data to evaluate the luminous efficiency factor. The present results are a refinement of a previously published analysis since new information on the properties of meteoritic materials has been utilized. A method has also been found for taking into account a delay in light production resulting from the time required to vaporize chunks of froth in the meteor wake.

The introduction of a frothing ablation model in an analysis of super-Schmidt meteor data allows an interpretation in terms of originally solid meteoroids for meteors previously thought to have been produced by fragile low-density meteoroids. At the same time, the computed luminous efficiency factor, τ_{op}, is found to vary substantially with velocity. Above 35 km/sec the value of τ_{op} is close to that recommended by Verniani. As the velocity is reduced below 25 km/sec τ_{op} increases to a level about six times greater.

INTRODUCTION

The fragmentation concept was originated in 1955 by Jacchia (ref. 1) as an explanation of the deceleration anomaly of faint meteors. The idea was supported by Whipple's earlier conclusion that cometary meteoroids were probably porous and fragile (see ref. 2). This view was widely accepted and attempts have been made to predict the behavior of such objects in the atmosphere, for example, Öpik's dust ball theory (ref. 3).

An alternative explanation of the observed anomalous decelerations and low densities was presented in reference 4. The explanation is based on results of ground-based arc-jet tests where it was shown that many materials, including those found in meteorites, develop low-density froths under conditions of high heating rates and low pressures. Frothing can result either from boiling of the melted material or expansion of volatile components contained in the melt. It can be concluded from these tests that a sample from an ordinary stone meteorite weighing one gram or less, if impelled into the upper atmosphere at meteoric velocity, would develop a shell of low-density froth. The mean density would thereby be lowered and could decrease during the trajectory, leading to an anomalously large deceleration. Although this

finding does not preclude the possibility that low-density porous meteoroids exist in space, it weakens some of the arguments that originally led to that hypothesis.

The view that a majority of meteoroids may be solid rather than porous, suggested in reference 4, was based in part on a mathematical model for the behavior of such meteoroids during ablation. The model was applied to an analysis of super-Schmidt meteor data to determine values of the luminous efficiency factor τ_{op} and the mean meteoroid density ρ_m. Previous meteor analyses that do not include a model for the ablation process can only predict the value of the ratio τ_{op}/ρ_m^2. The level of τ_{op} computed from data contained in reference 5 compared favorably with previous estimates. However, in contrast to the prevailing assumption (see, e.g., refs. 5 to 8) the luminous efficiency factor was found to increase with decreasing velocity rather than remaining constant over the entire range of meteor velocities. The predicted velocity dependence of the meteoroid flux in space is modified if τ_{op} is variable rather than constant. It was shown in reference 4 that the resulting modification leads to a better agreement with velocities predicted from overlapping radar data.

The present report explains the details of the mathematical model used for analyzing meteor data in reference 4. It also improves the model by including laboratory measurements of the properties of meteoritic materials. A method has also been found for taking into account a delay in light production when froth is sloughed off in relatively large pieces. It is shown that this delay is partially responsible for apparent increases of luminous efficiency along a trajectory. The evidence in support of the frothing-sloughing ablation model is thereby strengthened.

SYMBOLS

A meteoroid frontal area

A_f froth particle frontal area

A_{rn} geometric parameter in ablation model (eq. (A10))

A_{rs} geometric parameter in ablation model (eq. (A2))

A_s frontal area of solid inner core

B fraction of mass ablated as froth (eq. (19))

C heat-transfer parameter (eq. (C3))

C_D drag coefficient

C_F skin-friction coefficient

C_{Fu}	uncorrected skin-friction coefficient
C_H	aerodynamic heat-transfer coefficient
C_{Hcvu}	convective heat-transfer coefficient
C_{Heu}	equilibrium radiative heat-transfer coefficient
C_{Huu}	nonequilibrium radiative heat-transfer coefficient
C_{Hu}	uncorrected heat-transfer coefficient
C_μ	parameter in viscosity law (eq. (B11))
c_1, c_2	parameters in vapor pressure law (eq. (C11))
$\cos Z_R$	cosine of angle between meteor path and the vertical
F	factor (eq. (D8))
G	correction factor to account for nonlinear velocity profile
g_1, g_2, g_3	factors to allow for nonlinearities and nonuniformities in the viscous flow of the melt
h	instantaneous meteor altitide
I_p	photographic luminous intensity
i	parameter in viscosity law (eq. (B11))
k	thermal conductivity
l_f	length of cylindrical froth shell (fig. 18)
l_s	length of cylindrical solid core (fig. 18)
M	molecular weight of vapor
m	meteoroid mass
$\dot{m}$	rate of ablation of meteoroid mass with time
m_1	meteoroid mass based on τ_{opl}
m_f	mass of froth particle in wake
m_l	mass of liquid drop in wake
m_s	mass of solid inner core

3

$\dot{m}_s$ — rate of melting of solid core with time

P_v — heat-transfer parameter (eq. (C3))

$p_v, p_v(T)$ — equilibrium vapor pressure

Q — meteoroid total volume

Q_s — volume of solid inner core

R — ratio (eq. (12))

r — radius of meteoroid frontal area

r_f — radius of froth particle in wake

r_l — radius of liquid drop in wake

r_n — nose radius

r_s — radius of frontal area of solid core

S_F — shape factor (eq. (4))

S_{Fh} — shape factor of hemisphere, $\left(\dfrac{9\pi}{4}\right)^{1/3}$

T — meteoroid surface temperature at stagnation point

T_f — temperature of fusion

t — time

u — tangential velocity of melt

u_c — tangential surface velocity of melt at control surface

V — meteoroid velocity

$\dot{V}$ — meteoroid acceleration

$\dot{y}$ — rate of recession of solid surface at stagnation point

α — heat-transfer parameter (eq. (C3))

ΔL — lag distance of froth in meteoroid wake (eq. (22))

δ_c — thickness of melted layer at control surface

ϵ — surface emissivity

ζ — specific heat of ablation

ζ_f specific heat of fusion (latent plus stored)

ζ_v specific heat of vaporization (latent plus stored)

θ intensity lag time

θ_f time to ablate froth particle to nothing in wake

θ_l time to vaporize liquid drop

μ viscosity of solid

μ_f viscosity of froth

ρ air density

$\bar{\rho}$ ratio of air density to sea-level air density

ρ_o sea-level air density

ρ_{21} density ratio across normal shock

ρ_m meteoroid mean density

$\dot{\rho}_m$ rate of change with time of meteoroid mean density

ρ_{mf} froth density

ρ_{ms} solid density

σ Stefan-Boltzmann constant

σ_1 heat-transfer parameter (eq. (C3))

τ_{op} luminous efficiency factor (zero mag-cgs)

τ_{op1} assigned constant luminous efficiency factor (6.46×10^{-19} zero mag-cgs)

τ_{opc} corrected luminous efficiency factor

τ_p luminous efficiency (dimensionless)

τ_s surface tension

ω rate of vaporization per unit area

$\tilde{\omega}$ total rate of ablation per unit area due to evaporation and explosive spalling

ω_d rate of vaporization per unit area in a viscous boundary layer

ω_{FM} rate of vaporization per unit area in a vacuum

ω_s rate of melting of solid core mass per unit area and time (eq. (A14))

Subscripts

f   final point on trajectory (also froth)

i   integer denoting a point on a meteor trajectory

j   integer representing the number of iterations

$-\infty$ prior to entry into the atmosphere

ANALYSIS

In this section a set of relations will be exhibited that can be used to derive values of the luminous efficiency factor τ_{op} from meteor data. These relations are, in part, based on an ablation model which takes into account the production and viscous flow of froth in the heated region at the front of a meteoroid.

Basic Meteor Equations

In reference 5, meteor data, reduced from photographic data by the methods described in references 9 and 10, are presented as values at several points on the trajectories of each meteor of the following quantities:

h   altitude

m_1 mass

V   velocity

$\dot{V}$ acceleration

An identifying trail number and a value of $\cos Z_R$, the cosine of the angle between the meteor trajectory and the vertical, are given for each meteor. Much additional information, not of direct concern here, is included. The values of mass m_1 are based on an assumed constant value of the luminous efficiency factor

6

$$\tau_{op1} = 6.46 \times 10^{-19} \qquad (\text{zero mag-cgs})[1]$$

and a final mass equal to zero.

The luminosity and dynamic equations used in reference 5 are

$$I_p = -\frac{1}{2} \tau_{op} V^3 \frac{dm}{dt} \qquad (\text{luminosity equation})[1] \tag{1}$$

and

$$\dot{V} = -\frac{1}{2} C_D \frac{A}{m} \rho V^2 \qquad (\text{dynamic equation}) \tag{2}$$

At the outset, we shall take the masses in these two relations to be equal as in references 2 to 8. However, an alternative assumption allowing for a lag in the time required for light to be produced from froth particles in the wake is investigated and found to have merit.

The values of mass m_1 in reference 5 are based on the assumed luminous efficiency factor τ_{op1} and in accord with an integral of equation (1). The values of mass can be converted to correspond to a different luminous efficiency factor τ_{op} by integration backward along the trajectory using the relation

$$m = \int_0^{m_1} \frac{\tau_{op1}}{\tau_{op}} \, dm_1 \tag{3}$$

derived from equation (1). If τ_{op} is assumed to be constant between points on the trajectory, the integral in equation (3) can be replaced by a sum.

As in references 4 and 7 we shall assume that the shape of the meteoroid remains similar as it ablates during entry. Then the shape factor will be a constant and is expressed as

$$S_F = A/Q^{2/3} \tag{4}$$

where Q is the meteoroid volume given by

$$Q = m/\rho_m \tag{5}$$

---

[1]The units used in this report for all equations except the luminosity equation (1) are MKS. In the discussions, other units, such as grams and kilometers per second, may be specified. The units in the luminosity equation are those of reference 5. The photographic intensity I_p is expressed in units of the intensity of a zero magnitude star. The unit of the luminous efficiency factor τ_{op} is zero magnitude $\sec^4 \text{gram}^{-1} \text{cm}^{-3}$, abbreviated as zero mag-cgs. For use in other equations, the mass determined from equation (1) is multiplied by 10^{-3} to convert to MKS units. Methods for expressing the luminous efficiency in other forms that appear in the literature are considered in a later section.

in terms of the mass m and the meteoroid mean density ρ_m. From equations (2), (4), and (5) the mean density of the meteoroid can be expressed as

$$\rho_m = \frac{1}{\sqrt{m}} \left(-\frac{S_F C_D \rho V^2}{2\dot{V}} \right)^{3/2} \tag{6}$$

In this report, values of the air density ρ corresponding to the altitudes given in the data of reference 5 will be taken from reference 11. The meteoroid front face will be assumed to be a segment of a sphere and the drag coefficient C_D evaluated according to reference 12.

It can be seen that application of equations (3) and (6) to the reduced meteor data of reference 5 leads to evaluation of the ratio $S_F^3 \tau_{op}/\rho_m^2$ at each point on the trajectories where values of h, V, $\dot{V}$, and m_1 are given. Furthermore, if values for the shape factor S_F and meteoroid density ρ_m are assumed as in reference 6, the luminous efficiency factor τ_{op} can be evaluated. Alternatively, an additional relation involving these quantities can be arrived at by consideration of the ablation process occurring during atmospheric flight as in references 7 and 13. The ablation model developed for this purpose in the present report differs from those previously employed in that it takes into account the frothing and sloughing of meteoritic materials as observed in arc-jet tests. Application of this model to reduced meteor data from reference 5 leads to evaluation of τ_{op} and ρ_m individually as well as the ratio τ_{op}/ρ_m^2 resulting from previous analyses. For that purpose it remains necessary to assume a value for the shape factor S_F, but the effect on the results of variations in this quantity is investigated.
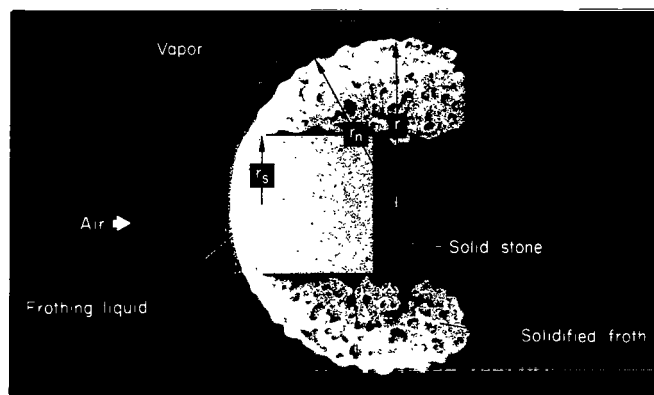

Figure 1.- Sketch of the cylinder (solid) hemisphere (froth) assumed in the meteoroid ablation model.

Ablation Model

The arc-jet tests on which our model is based are described in references 4 and 14. Figure 1 illustrates the processes observed in the tests, which we assume also occur in meteor flight. The solid stone core melts at the front face and runs to the side with only a small amount of vaporization. Upon reaching a region of low enough pressure, the melted stone froths. The frothing can be caused by volatile components in the melt, or, in the absence of such components, by boiling. After reaching the sides, where the heating from the air is less severe, the froth solidifies. Chunks of froth intermittently break off and, in the case of a meteor, are assumed to undergo further ablation and eventually vaporize in the wake. In a part of the range of test conditions covered, the froth ran off the model in the liquid form rather than solidifying. This occurred at conditions corresponding to the later parts of slow meteor trajectories.

Since the tests were run under conditions that did not correspond completely to meteor flight, a discussion of the differences is in order. The heating loads and impact pressures of the tests corresponded to slow (15 km/sec) meteors at altitudes from 70 to 100 km. The effective altitude was held constant in each test, and acceleration effects were not simulated. Models made of material taken from stone and iron meteorites were tested and found to react in the same manner as similar terrestrial materials. The models were originally round-nosed cylinders with a radius of 1 cm, weighing about 30 grams. Tests as long as 115 seconds were required at the higher effective altitudes to achieve the conversion of an appreciable fraction of the material to froth. It is important to note that frothing is a surface phenomenon rather than one that occurs throughout the volume of the solid material. Therefore, frothing of the same fraction of mass will occur in a shorter time in a smaller object. For example, if the time required for melting a given fraction of the mass is taken to be proportional to the ratio of volume to surface area, the same degree of melting would occur in a 1 gram mass in one-third the time required for a 27-gram mass. Therefore, the fraction of a 30-gram model converted to froth in 115 seconds at an altitude of 98 km would correspond to a test time of about 36 seconds for a 1-gram mass at the same altitude. Since the heat load is approximately proportional to air density, the same degree of frothing would be expected in 3.6 seconds in a 1-gram mass at an altitude of 86 km where the air density is about 10 times greater than at 98 km. This forms a part of the basis of our assumption that meteoroids in the mass range below 1 gram will undergo a degree of frothing comparable to that observed in the tests.

The effective velocity of the tests (about 15 km/sec) corresponds to the velocity of slow meteors. Since the heating is approximately proportional to the cube of velocity, an increase in velocity by a factor of 3 would decrease the time required for melting at a given altitude by about a factor of 27. Therefore, a fast meteor below 1 gram in mass receives sufficient heat to froth at altitudes above 98 km. It is possible that other effects not observed in the tests would occur at velocities above those reached. For example, vaporization might take place rapidly enough to prevent the degree of froth build-up observed in the tests. We do not have direct evidence to rule out this possibility. However, the calculations to be discussed later in this report indicate that for all of the meteors analyzed most of the solid material at the front face is removed by viscous flow of the melted material, rather than by vaporization. Our conclusion from this is that the eventual vaporization of meteoroids of this size takes place largely in the wake rather than on the parent meteoroid. An important link in this reasoning is the finding that, at the temperatures involved, the viscosity of meteoritic stone (and similar terrestrial materials) is several orders of magnitude lower than that of a glass with high silicate content.

The major assumptions utilized in the ablation model are as follows:

1. The meteoroid front face, comprised partly of froth and partly of a thin layer of melted material covering the solid core, remains shaped as the surface of a segment of a sphere with the radius of the frontal area r a constant fraction of the nose radius r_n during ablation.

2. The ratio of solid volume to total volume Q_s/Q is proportional to the cube of the ratio of the frontal area radii r_s/r (see fig. 1).

3. During ablation the spherical front face of the solid remains centered in the froth and the entire front face remains oriented with respect to the airstream as shown in figure 1.

4. Ablation of the solid material takes place by vaporization and viscous flow with negligible effects from surface undulations such as ring waves (ref. 15). The solid core does not fragment.

5. The solid core is composed of a meteoritic material for which the properties such as thermal heat conductivity, viscosity, etc., are known.

The origin and implications of the assumptions are discussed in appendix A. The viscous flow of melted material resulting from the impinging airstream is analyzed only for the thin layer covering the front of the solid core. The ablation model based on the foregoing assumptions is thus in a sense incomplete in that no attempt is made to predict the degree of froth build-up or to follow the mode of ablation of the froth (whether by vaporization, viscous flow, or fragmentation). Instead, the degree of froth accumulation is deduced from the meteor data with the aid of the foregoing assumptions plus those implicit in the basic meteor equations. The geometric assumptions are made in lieu of an attempt to guess the original shape and predict evolutions of shape from a detailed study of the ablation processes occurring.

An expression for the rate of melting of solid core mass per unit area and time is derived in appendix A in the form

$$\omega_s = -\frac{1}{A_{rs}^2 S_F}\left(\frac{\rho_m}{m}\right)^{2/3}\left[\frac{\rho_{ms}}{\rho_m}\left(\frac{\rho_m - \rho_{mf}}{\rho_{ms} - \rho_{mf}}\right)^{1/3}\dot{m} + \frac{m\rho_{ms}\rho_{mf}}{(\rho_m - \rho_{mf})^{2/3}(\rho_{ms} - \rho_{mf})^{1/3}\rho_m^2}\dot{\rho}_m\right]$$

(7)

where

A_{rs} geometric parameter that determines the radius of the solid frontal area relative to the radius of the total frontal area

S_F shape factor

m meteoroid mass

ρ_m mean meteoroid density

ρ_{mf} density of froth

ρ_{ms} density of solid core

The rate of melting of solid mass per unit area is related to the values and derivatives of the meteoroid mass and mean density by this equation when
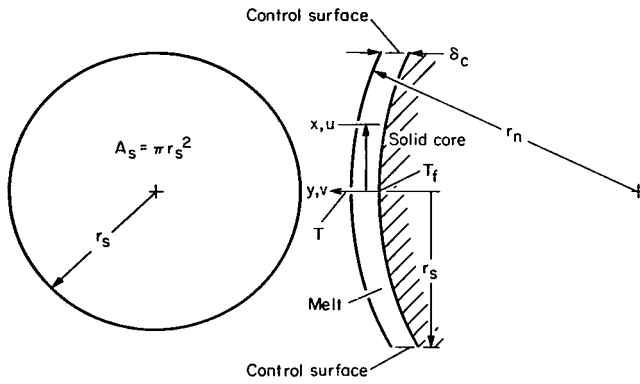
Figure 2.- Coordinate system for the viscous flow of the melt in the thin layer at the front of the solid core.

the parameters A_{rs}, S_F, ρ_{ms}, and ρ_{mf} are assigned. The values of the parameters used for most of the calculations are listed in table I, but the effects on the results of reassignment of the values will be considered.

In appendix B, equations are derived that express the conservation of mass, momentum, and energy for the viscous flow of the thin layer of melted material at the front of the solid core. Figure 2 indicates that part of the meteoroid under consideration. The relations derived in appendix B are combined to form the equation

$$\left(\frac{k}{\zeta_f}\right)^2 \frac{\rho_{ms}}{\mu(T)} (T - T_f)^2 G(T) = \frac{A_{rn}S_F^{1/2} \left(\frac{m}{\rho_m}\right)^{1/3} (\omega_s - \tilde{\omega})}{\sqrt{\pi}C_F\rho V^2} \tag{8}$$

where

k   thermal conductivity of melted meteoroid

ζ_f specific heat of fusion plus sensible heat

ρ_{ms} density of solid meteoroid core

$\mu(T)$ viscosity of melted meteoroid

T   stagnation-point surface temperature

T_f temperature of fusion of meteoroid

$G(T)$ correction factor for nonlinear velocity profile (appendix B)

A_{rn} ratio of nose radius to radius of frontal area

S_F shape factor

m   meteoroid mass

ρ_m meteoroid mean density

ω_s rate of melting of the meteoroid solid core per unit area and time (eq. (7))

$\tilde{\omega}$ rate of evaporation of solid core material per unit area and time (eq. (C12))

C_F tangential surface force coefficient

ρ air density

V meteor velocity

The material property laws assumed and the aerodynamic laws utilized are discussed in appendixes B and C. Most of the results in this report are based on material properties appropriate for carbonaceous chondrites. However, the effect on the results of variations in properties is investigated.

If the quantities appearing in the auxiliary relations are considered evaluated, substituting equation (7) into (8) would lead to a complicated expression which can be indicated symbolically as

$$F(\dot{m}, m, \dot{\rho}_m, \rho_m; h, V, \dot{V}) = 0 \tag{9}$$

This ablation equation provides an additional relation between the quantities appearing in the basic meteor equations. It can be seen that insertion of values of h, V, and $\dot{V}$ from reduced meteor data into equation (6), a form of the dynamic equation, and the ablation equation (9) leads to evaluation of m and ρ_m along the meteor trajectory. That information plus the values of m_1 from the reduced meteor data can be used in equation (3), a form of the luminosity equation, to determine the luminous efficiency factor τ_{op}. As a result of this procedure, values of both τ_{op} and ρ_m are obtained (only the ratio τ_{op}/ρ_m^2 is found from the use of the luminosity and dynamic equations without an ablation equation).

Method of Solution

An iterative procedure is used for the calculation of values of τ_{op} and ρ_m at each point on the trajectory of a meteor where values of h, V, $\dot{V}$, and m_1 are given in reference 5. A computer program has been developed for that purpose. The computations performed in each stage of the iteration are indicated in the following numbered paragraphs.

1. The mass m along the trajectory is assigned the values from the previous iteration, and equation (6) is used to compute ρ_m at each trajectory point.

The evaluation of $\dot{m}$ is based on the relation

$$\dot{m} = -V \cos Z_R \frac{dm}{dh} = -V \cos Z_R m \frac{d \ln(m)}{dh} \tag{10}$$

obtained with the aid of the trajectory relation

$$\frac{dh}{dt} = -V \cos Z_R$$

The logarithmic differentiation is employed because of the relative constancy of $d \ln(m)/dh$ compared to dm/dh along the trajectory. Similarly, the

evaluation of $\dot{\rho}_m$ is based on

$$\dot{\rho}_m = -V \cos Z_R \rho_m \frac{d \ln(\rho_m)}{dh} \tag{11}$$

The derivative $d \ln(m)/dh$ is approximated at midpoints between trajectory points by simple differences according to the relation

$$\left[\frac{d \ln(m)}{dh}\right]_{i+\frac{1}{2}} = \frac{\ln(m_{i+1}) - \ln(m_i)}{h_{i+1} - h_i}$$

where the subscript i denotes the ith trajectory point. A linear interpolation is used to compute derivatives at the trajectory points,

$$\left[\frac{d \ln(m)}{dh}\right]_i = \left(\frac{h_{i+1} - h_i}{h_{i+1} - h_{i-1}}\right) \left[\frac{d \ln(m)}{dh}\right]_{i-\frac{1}{2}} + \left(\frac{h_i - h_{i-1}}{h_{i+1} - h_{i-1}}\right) \left[\frac{d \ln(m)}{dh}\right]_{i+\frac{1}{2}}$$

The derivative $d \ln(\rho_m)/dh$ is evaluated by the same method. This method is not applicable at the first and last trajectory points, which are therefore dropped from the subsequent calculations. For that reason, only meteors with data given for at least three trajectory points can be used in our machine program in its present form.

2. The quantities $\dot{m}$ and $\dot{\rho}_m$ along the trajectory are evaluated (eqs. (10) and (11)) using the numerical procedure described above.

3. Values of ω_s are computed by means of equation (7).

4. The stagnation-point temperature T and the quantities $\mu(T)$, $G(T)$, $\tilde{\omega}$, and C_F in equation (8) are computed with the aid of auxiliary relations given in appendixes A, B, and C.

The viscous flow equation (8) is redundant in terms of the quantities computed in the previous steps. Therefore, it can be used to readjust the values of mass that were assigned at the beginning. For that purpose the ratio of the two sides of equation (8)

$$R = \frac{A_{rn} S_F^{1/2} \left(\frac{m}{\rho_m}\right)^{1/3} \omega_s^2 (\omega_s - \tilde{\omega})}{\sqrt{\pi} C_F \rho V^2 \left(\frac{k}{\zeta_f}\right)^2 \frac{\rho_{ms}}{\mu} (T - T_f)^2 G(T)} \tag{12}$$

serves as an indicator of the needed change. By trial and error it has been found that if R is not equal to 1, as it should be, readjusting the luminous efficiency factor according to the relation

$$\tau_{op_j} = R^{1/2} \tau_{op_{j-1}} \tag{13}$$

13

will give a value of R closer to 1 in the next iteration. The subscripts j and j-1 refer to the jth and (j-1)th iterations, respectively.

5. The next step in the calculation is the evaluation of R and τ_{op} at each point of the trajectory (except the first and last points) using equations (12) and (13).

6. Equation (3) can now be used in the form

$$m_{ji} = \left(\frac{\tau_{op_{j-1}}}{\tau_{op_j}}\right)_i (m_{j-1,i} - m_{j-1,i+1}) + m_{j,i+1} \tag{14}$$

to compute the adjusted values of mass along the trajectory. The subscript j refers to the stage of the iteration and the subscript i to the point on the trajectory. For the final point on the trajectory, the relation

$$m_{jf} = \left(\frac{\tau_{op_{j-1}}}{\tau_{op_j}}\right)_{f-1} m_{j-1,f} \tag{15}$$

is used, where the subscript f-1 refers to the next to last point. The luminous efficiency factor for the last point is not computed because of failure at that point of the method of numerical differentiation employed in step 2.

After completion of step 6, new values of mass along the trajectory are available for use in the next iteration starting with step 1. For most of the reduced meteor data from reference 5 treated in this report, 10 iterations lead to values of R that differ from 1 by less than 10 percent. It has been found that the resulting values of m, ρ_m, and τ_{op} along the trajectory are independent of the luminous efficiency factor assumed at the beginning of the iteration to provide starting values of the mass.

In the discussion following equation (9), it was stated that values of mass m and mean meteoroid density ρ_m could be derived from the meteor data with the aid of the dynamic and ablation equations without reference to the luminosity equation. That purpose can be accomplished in the foregoing iteration procedure by merely declining to identify the quantity τ_{op} computed in equation (13) as the luminous efficiency factor. In that case, equation (14) can be regarded as one of the mathematical steps in the iteration procedure rather than identifying it with the luminosity equation. Therefore, if modifications of the luminosity equation are considered, it is not necessary to change equation (14) or any part of the iteration procedure. The values of mass and meteoroid density computed from the iteration are thereby determined from the dynamic and ablation equations alone. They can therefore be used in a modified form of the luminosity equation to determine a luminous efficiency factor τ_{opc} that is not equal to the dummy variable τ_{op} used in the iteration. We shall have occasion later in this report to make use of this observation in investigating the effects of a lag in the time required for light production from froth particles in the meteor wake. However, first we shall

14

consider the predictions of the model based on the conventional luminosity equation. In that case the values of τ_{op} computed in equation (13) are identified as the luminous efficiency factor defined by equation (1) or (3).

Statistical Procedure

The iterative procedure for analyzing meteor data described in the previous section can be used to compute quantities such as the luminous efficiency factor, meteoroid density, and mass along the trajectories of individual meteors. A machine program has been developed for this purpose and applied to 40 of the meteors for which data are given in reference 5. The trail numbers of the 40 meteors are listed in table II. Values of the luminous efficiency factor so obtained vary by more than an order of magnitude. As discussed in references 5 and 6, there are a number of sources of random error that render the data of individual meteors unreliable. Consequently, the authors of those references recommend the use of statistical methods to analyze the data of a number of meteors simultaneously.

In the method adopted here the calculations described in the previous section are carried out for individual meteors and subsequently statistical analyses are made of the resulting values of quantities such as the luminous efficiency factor. Our machine program was expanded to include such processes. Tables are formed of the computed and input quantities for all of the meteors in the sample. The tables are rearranged in the order of increasing velocity. A least squares fit to a straight line is then made of the logarithm of the luminous efficiency factor as a function of velocity and the root-mean-square deviation computed. This operation is carried out in subintervals of the total velocity range since the resulting velocity dependence is not linear over the entire range. Figure 3 is an example of the results from such a
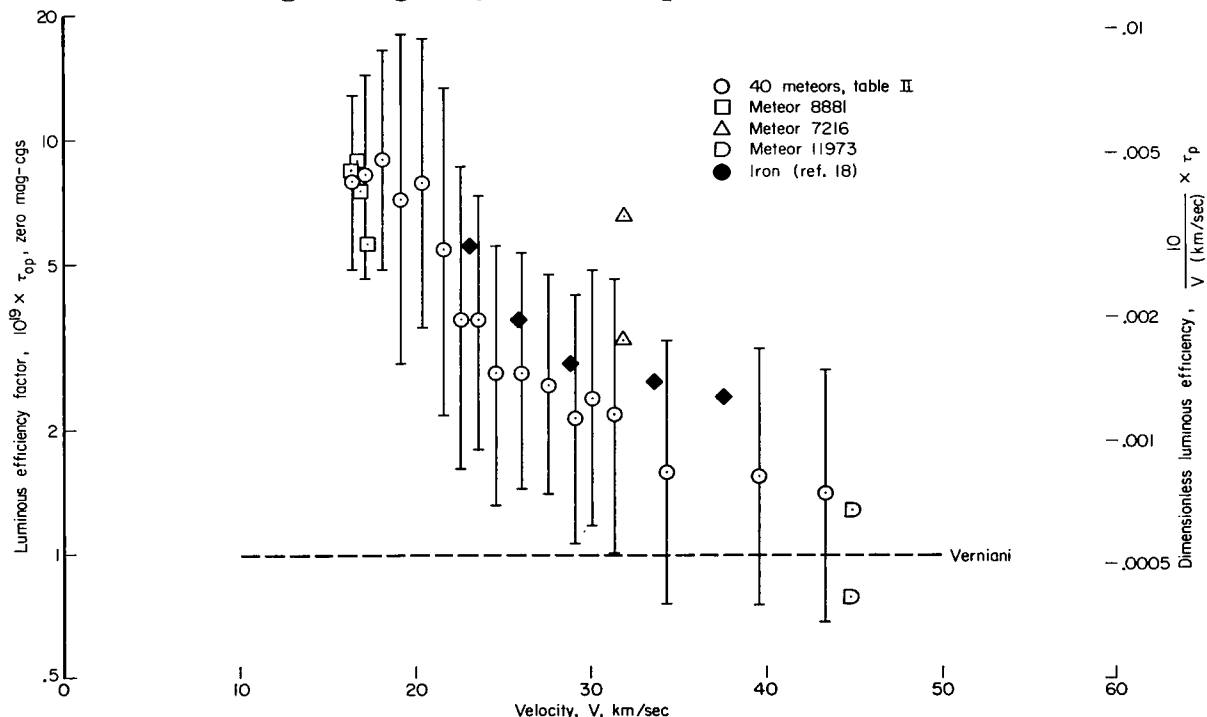

Figure 3.- Luminous efficiency factor versus velocity.

15

calculation. The circles are the values of the luminous efficiency factor from the least squares fit at the mean velocity in the subinterval of velocity covered in each case. The vertical bars indicate the root-mean-square deviation. Each circle in figure 3 is computed from 20 trajectory points from about 10 meteors (more or less, depending on the number of trajectory points per meteor). It should be mentioned that each circle in figure 3 does not represent an independent set of data. Adjacent circles represent two groups of data that have 15 trajectory points in common out of their totals of 20 points each. Thus only every fourth circle represents independent data. The overlapping was employed to obtain a better indication of the velocity dependence from a limited amount of data.

In other operations, the tables of computed and input quantities are arranged in the order of increasing mass or impact pressure instead of velocity. Least squares fits are then made in subintervals of the ordered variable to construct plots of luminous efficiency factor versus mass and versus impact pressure as shown in figures 4 and 5. Least squares fits and plots of other quantities such as mean meteoroid density are also made as shown in subsequent figures.

A 40-meteor sample was selected from among those available in reference 5 for the foregoing operations. The selection was made on the basis of the longest trails and a wide velocity range. Several meteors for which the program indicated densities greater than iron or very large luminous efficiencies were replaced by others. The trail numbers of the final 40-meteor sample are listed in table II.

It is stated in reference 5 that the 413 meteors for which reduced data are given do not represent a random sample of the incoming meteoroid flux. For example, the relative numbers in a given magnitude range drop below that of larger samples in the faint meteor range. The corresponding distribution of our 40-meteor sample is similar to that of the 413 meteors of reference 5, although it is more erratic because of the small number involved. The bias against faint meteors is amplified also because long trails were selected. The photographic magnitude range encompassed in our sample is +1.8 to -3.6. The computed preentry masses lie between 0.0828 and 3.30 grams. For spheres of density 2.8 gm/cm^3, the corresponding radii are 0.19 to 0.65 cm. The computed radius of the hemispherical froth shell developed during flight in the atmosphere averages about 0.7 cm.

RESULTS AND DISCUSSION

Results From Statistical Procedure

As mentioned in the previous section, the results from an analysis of super-Schmidt meteor data are presented in figure 3. The scale on the left indicates the units used in references 5 and 6 for the luminous efficiency factor τ_{op}. The scale on the right can be used to compute the equivalent dimensionless luminous efficiency τ_p, which is the fraction of the kinetic energy of the vaporized atoms that is converted to light detectable by the
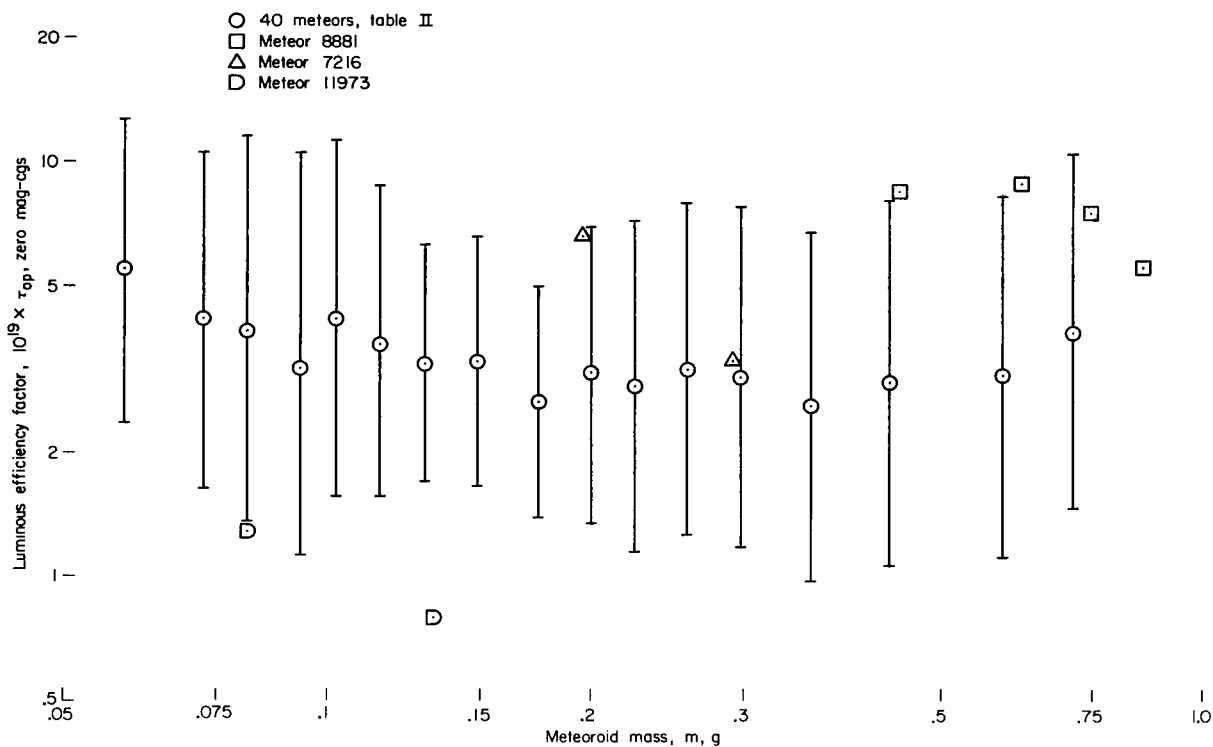
Figure 4 (top):

O 40 meteors, table II
□ Meteor 8881
△ Meteor 7216
Ð Meteor 11973

20 —

10 —

5 —

2 —

1 —

Luminous efficiency factor, $10^{19} \times \tau_{op}$, zero mag-cgs

Ð

.5 L
.05   .075   .1   .15   .2   .3   .5   .75   1.0

Meteoroid mass, m, g

Figure 4.- Luminous efficiency factor versus meteoroid mass.

Figure 5 (bottom):

O 40 meteors, table II
□ Meteor 8881
◇ Meteor 6949
△ Meteor 4464

20 —

10 —

5 —

2 —

1 —

Luminous efficiency factor, $10^{19} \times \tau_{op}$, zero mag-cgs

.5 L
500   750   1000   1500   2000   3000   5000   7500   10,000
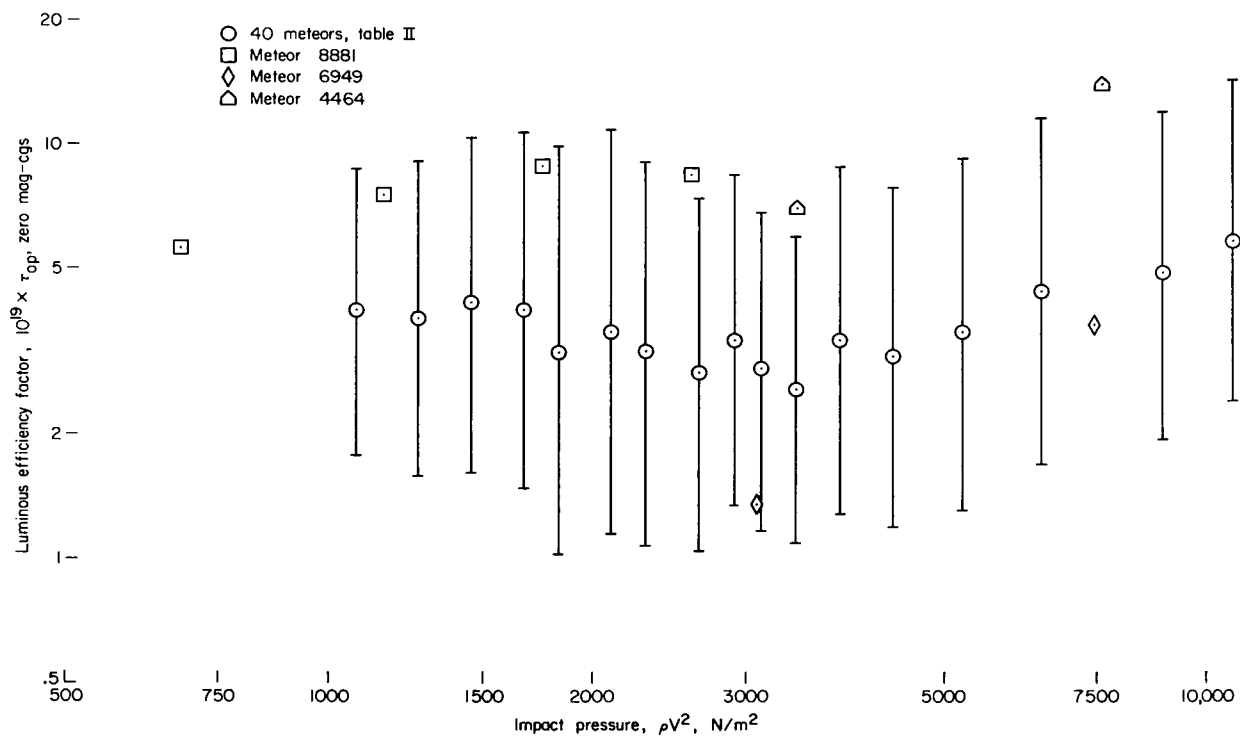
Impact pressure, ρV^2, N/m^2

Figure 5.- Luminous efficiency factor versus impact pressure.

17

blue sensitive film used in the super-Schmidt cameras. This scale was constructed according to reference 6. Additional information on the method of conversion is contained in references 16 and 17. Since the quantity read from the scale is $10\tau_p/V$, it should be multiplied by $V/10$ to obtain the luminous efficiency τ_p.

Even though updated material properties have been used, figure 3 is still similar to that from the preliminary analysis reported in reference 4. The constant value of τ_{op} recommended by Verniani in reference 6 is shown as a dashed line in the figure. The values of τ_{op} from the present method approach Verniani's value at high velocity, but rise with decreasing velocity rather than remaining constant. It was shown in reference 4 that such a velocity dependence of τ_{op} brings the velocity dependence of the meteoroid flux deduced from photographic meteor data into better agreement with overlapping radar results. A similar velocity dependence of τ_{op} was found for small iron spheres in laboratory experiments (ref. 18). Averages over 10 points at a time of the 50 data points given in reference 18 are shown in figure 3. The necessary conversion of units was based on the assumption that the luminous efficiency measured in the experiments was the photographic efficiency τ_p. According to reference 8 the luminous efficiency for stone should be less than that for iron by a factor of about 6.5. No readjustment in the results shown for iron has been made to convert to an equivalent value for stone.

Values of τ_{op} versus V for three individual meteors are included in figure 3 to show typical variations along a trajectory. The individual meteors in the present sample cover a relatively small velocity range, but the values of τ_{op} computed often vary by more than a factor of 2 along a trajectory.

It is known that, due to instrument selection effects and other factors, correlations exist between variables such as mass and velocity in meteor data chosen at random (ref. 5). It is therefore of interest to determine whether the apparent velocity dependence of τ_{op} shown in figure 3 might be basically a dependence on mass or other variables. Figure 4 is a plot of τ_{op} versus mass. It appears that the correlation with mass is less than with velocity. Typical variations along the trajectory are shown for three individual meteors in figure 4.

Figure 5 is a plot of τ_{op} versus impact pressure, ρV^2, constructed from the same meteor data as the previous two figures. It appears that there is little or no correlation of τ_{op} with this variable for the 40 meteors used in the calculation. Typical results for three individual meteors shown in the plot indicate that the impact pressure can increase appreciably along a trajectory.

As explained in the Analysis section the present method of meteor analysis leads to a prediction of the variable mean meteoroid density along a trajectory. Figure 6 shows the mean meteoroid density as a function of impact pressure obtained by averaging over 20 trajectory points at a time. As discussed in the section on the statistical procedure, each average is constructed from the data of a number of meteors, depending on the number of
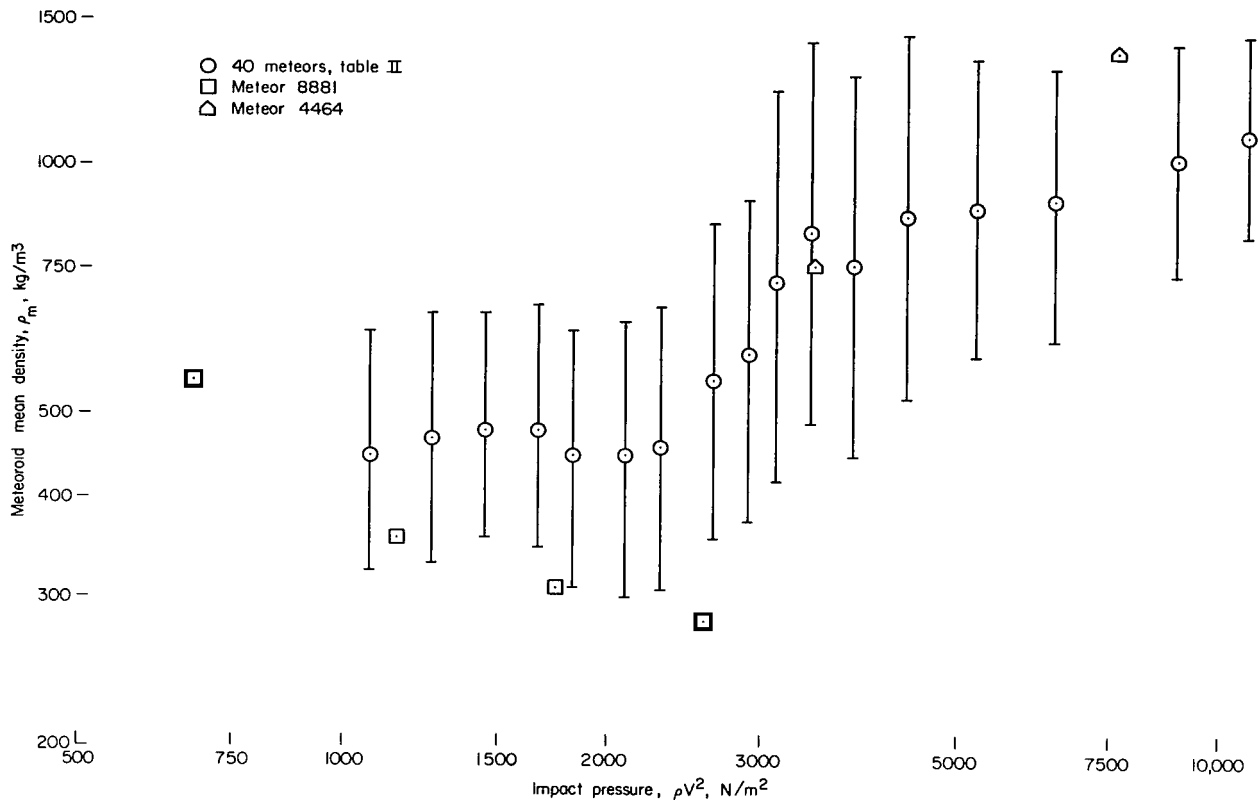
18

Figure 6.- Meteoroid mean density versus impact pressure.

trajectory points per meteor falling in the range of impact pressure included in the average. The computed values of mean meteoroid density versus impact pressure are also shown for two individual meteors in figure 6. The results for these two meteors indicate that both the mean meteoroid density and impact pressure vary appreciably along a trajectory.

Individual meteors either increase or decrease in density. However, the averages over several meteors shown in figure 6 indicate a systematic tendency toward higher mean meteoroid densities at the larger impact pressures. This indication of a smaller accumulation of froth on the average at higher impact pressures can be attributed to the greater likelihood of the froth being blown off. It would be difficult to explain this plot on the basis of meteoroids not containing solid inner cores. For example, a general fragmentation of fragile meteoroids should result in lower apparent densities at higher impact pressures, opposite to the tendency shown in figure 6. This observation lends credence to the assumption that the solid inner core does not fragment for a majority of meteors in the sample.
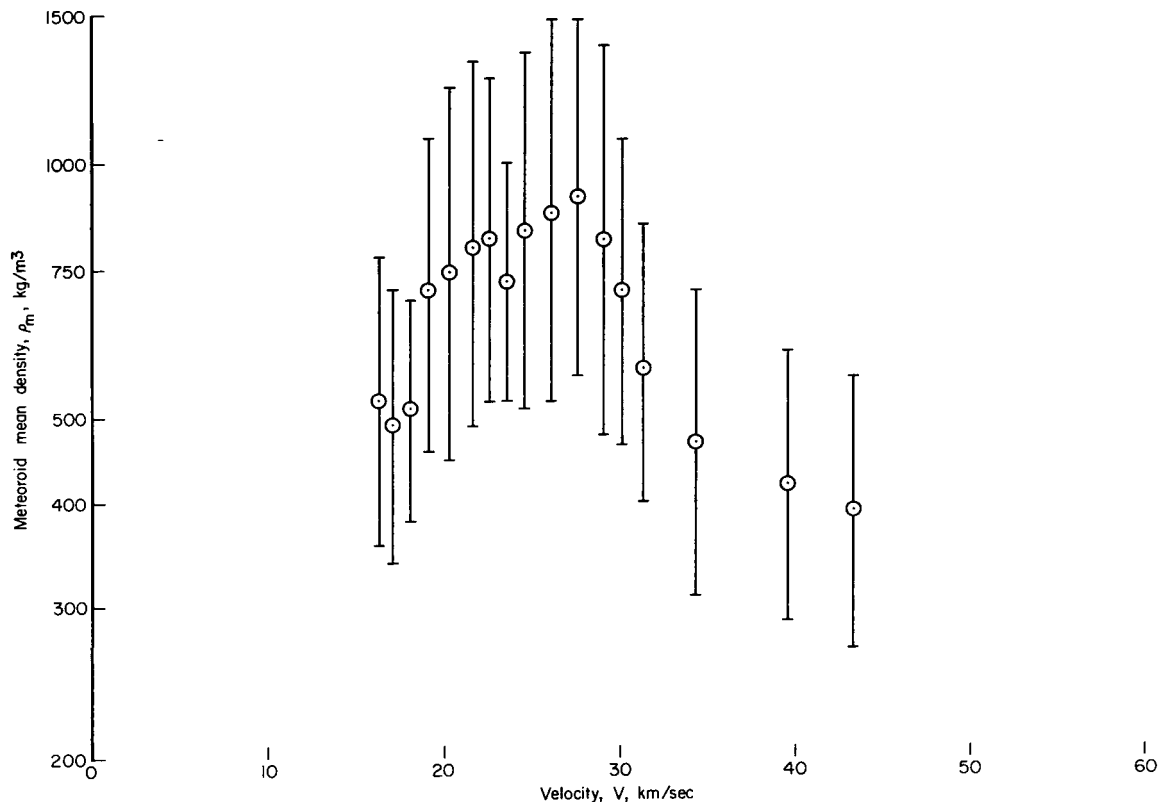
Figure 7.- Meteoroid mean density as a function of velocity.

Figure 7 shows the mean meteoroid density as a function of velocity. The correlation of density with velocity is less than the correlation with impact pressure shown in the previous figure in the sense that the scatter overlaps the variation more. The drop-off in mean density at high velocity can be related to the lower impact pressures experienced by the higher speed meteors on the average. The drop-off in mean density at lower velocity is believed to be fortuitous. An unexpectedly large fraction of the low velocity trajectory points in the sample occurred at values of the impact pressure less than 2000 N/m^2. According to figure 6, small values of mean meteoroid density are to be expected under such conditions. The depressed impact pressure at low velocity in our meteor sample is due to a combination of factors. About a third of such points correspond to early parts of the trajectories. For several of the meteors involved the later parts of the trajectories were truncated because they left the field of view of one of the observing cameras. The contributions of the larger mean densities that do occur at low velocity are suppressed in the logarithmic averages that include the more numerous trajectory points showing small mean densities.

In reference 6, Verniani reported an analysis of 360 of the meteors contained in reference 5. It was found that the average value of $\tau_{op} V/\rho_m^2$ for meteors with aphelia greater than 7 AU was greater by a factor of 2 than the average for those with smaller aphelia. The method of reference 6, based on the luminosity and dynamic equations, did not permit a determination of the mean density ρ_m alone. It was assumed that the effect was due to a difference in density of the two groups of meteoroids. The difference in density was justified on the basis of Whipple's icy comet model. No allowance was made for possible changes in mean meteoroid density due to frothing in the atmosphere. On this basis τ_{op} was found to be independent of velocity if the long-period meteoroids were assumed to be less dense by a factor of 1.4 than the short-period meteoroids. With no difference in density for the two groups, it was found that τ_{op} would be approximately proportional to $V^{1/2}$.

In the present method the mean meteoroid density and luminous efficiency factor are computed separately. With the aid of information contained in reference 19, it has been determined that the last three average values of mean meteoroid density on the right in figure 7 are largely from meteoroids in orbits with aphelia greater than 7 AU. Most of the meteoroids used for the averages at lower velocities are from orbits with aphelia less than 7 AU. If we ignore the decline in mean density at lower velocity for reasons previously discussed, a difference in mean density of about a factor of 2 is found for the two groups of meteoroids discussed by Verniani. If this density ratio were put into Verniani's analysis, the luminous efficiency factor determined would rise with decreasing velocity rather than remaining constant. As previously discussed, the decline in mean density at high velocity can be attributed to the greater froth accumulation that is possible at the lower impact pressures experienced rather than to a difference in the densities of the meteoroids before entry into the atmosphere. In a later section, the effect of changes in the assigned parameters is discussed. From that study it can be determined that if the density of the solid core were assumed to be smaller for long-period meteoroids than those with aphelia less than 7 AU, the decrease in mean meteoroid density at high velocity would be accentuated by about the same ratio. This would lead to an even faster rise in luminous efficiency with decreasing velocity from Verniani's analysis than would result from the density variation shown in figure 7. Likewise, if a lower density of the solid meteoroid core were assumed for high-velocity meteors, the luminous efficiency factor computed by the method of the present report would drop even more than with a constant solid core density (see eq. (16)).

A plot of mean meteoroid density versus mass showed little correlation and is not reproduced here. The most informative plot of mean density is considered to be that showing its dependence on impact pressure in figure 6, which was previously discussed.
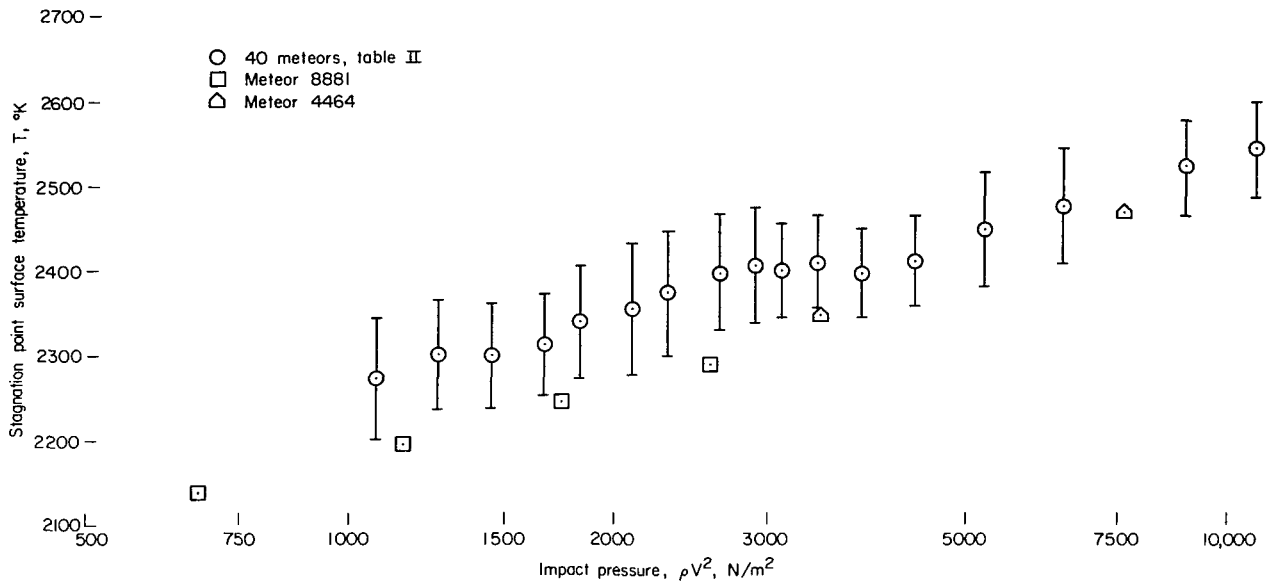
Figure 8.- Stagnation-point surface temperature versus impact pressure.

Plots have been made of computed values of the surface temperature at the stagnation point versus velocity, mass, and impact pressure. Of these, the one indicating the greatest correlation is the plot of temperature versus impact pressure shown in figure 8. The stagnation-point surface temperature would be a monotonic function of ρV^3 except for variations of the aerodynamic heat-transfer coefficient, which depends on the velocity, air density, and nose radius of the meteoroid. Allowing for evaporation of volatile meteoroid components in the aerodynamic energy equation (C2), discussed in appendix C, also disturbs this monotonic relationship. The scatter in figure 8 reflects these disturbing influences as well as the difference in velocity dependence of the impact pressure ρV^2 and the airstream energy flux ρV^3. Results for two individual meteors plotted in the figure show that the surface temperature and impact pressure increase appreciably along a trajectory.

Sensitivity of Results to Assumptions

Since the meteoroid properties are uncertain and an idealized meteoroid shape has been assumed in the foregoing analysis, it is of interest to determine the effect on the computed luminous efficiency factor of changes in assigned values of the parameters. For this purpose, it is helpful to derive approximate expressions for the dependence of τ_{op} on the parameters. The resulting approximations have been checked by making calculations for a few meteors with one parameter at a time varied. A matter of particular interest is to determine whether any reasonable change in assumed properties can remove the velocity dependence of the luminous efficiency factor indicated by the present method.

By means of approximations of equations (3), (7), and (8) described in appendix D, the proportionality relation

$$\tau_{op} \propto A_{rn}^{3/4} A_{rs}^{-9/2} S_F^{-15/8} \rho_{ms}^{3/2} \rho_{mf}^{-1/4} \tag{16}$$

has been derived. This expression indicates that if, for example, the assigned value of the nose radius parameter A_{rn} is doubled, the computed values of τ_{op} will be increased by the factor $2^{3/4} = 1.682$. This applies to the computed values at each point on the trajectory of an individual meteor as well as the averages from the statistical procedure. In figure 9 the above prediction is compared with the results of machine calculations for a few individual meteors.

Figures 10 and 11 show similar comparisons with respect to variations of the geometrical parameters A_{rs} and S_F. The shapes corresponding to these changes in parameters are discussed in appendix A and are depicted in figures 19 and 20. It can be seen from figures 9 to 11 that equation (16) is a reasonably accurate approximation in view of its simplicity. Since the magnitudes of the variations considered are in a range that can be expected to occur in a sample of meteors, it is clear that the level of the luminous efficiency factor determined in the previous section is not well determined. However, a systematic variation of the parameters with velocity that would remove the velocity dependence of the luminous efficiency factor appears unlikely.

The predictions of equation (16) with respect to changes in the assigned values of the density of the solid core and of the froth density are compared with results from machine calculations in figures 12 and 13. The approximation appears to be useful for adjusting the solid core density, but not the froth density. For the latter, the variations in the luminous efficiency factor are larger than predicted and are in the opposite direction. This failure has been traced to the step in the approximation whereby the second term in equation (7) is omitted (see appendix D). This term is ordinarily small compared to the first term, but increasing ρ_{mf} by a factor of 3 increases the ratio of the two terms by about the same factor so that the effect of the second term becomes more important. In addition, the term in question contains $\dot{\rho}_m$ as a factor which occasionally becomes large. For this reason, the machine calculations also become erratic when a large value is assigned to the froth density. It can be argued that large values of this term should be suppressed when they lead to increased scatter in the computed values of the luminous efficiency factor. The subject will not be pursued further here. However, it should be noted that if values of the froth density above about 200 kg/m^3 are of interest, complications not indicated by the approximate equation (16) should be considered.

Approximations leading to predictions of the effects of changes in other assigned parameters are described in appendix D. The proportionality relation

$$\tau_{op} \propto C_F^{-3/4} \left(\frac{k}{\zeta_f}\right)^{-3/2} C_{\mu}^{3/4} T_f^{-3/16} p_v^{3/8} \tag{17}$$
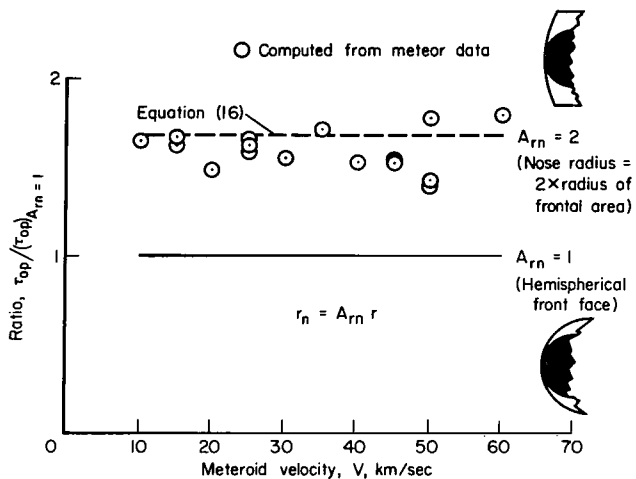
23

Figure 9.- Effect on computed luminous efficiency factor of nose bluntness.
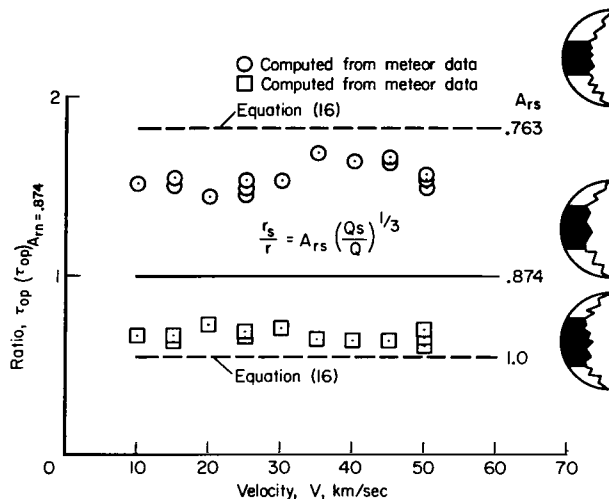

Figure 10.- Effect on luminous efficiency factor of changes in the geometric parameter A_{rs}.
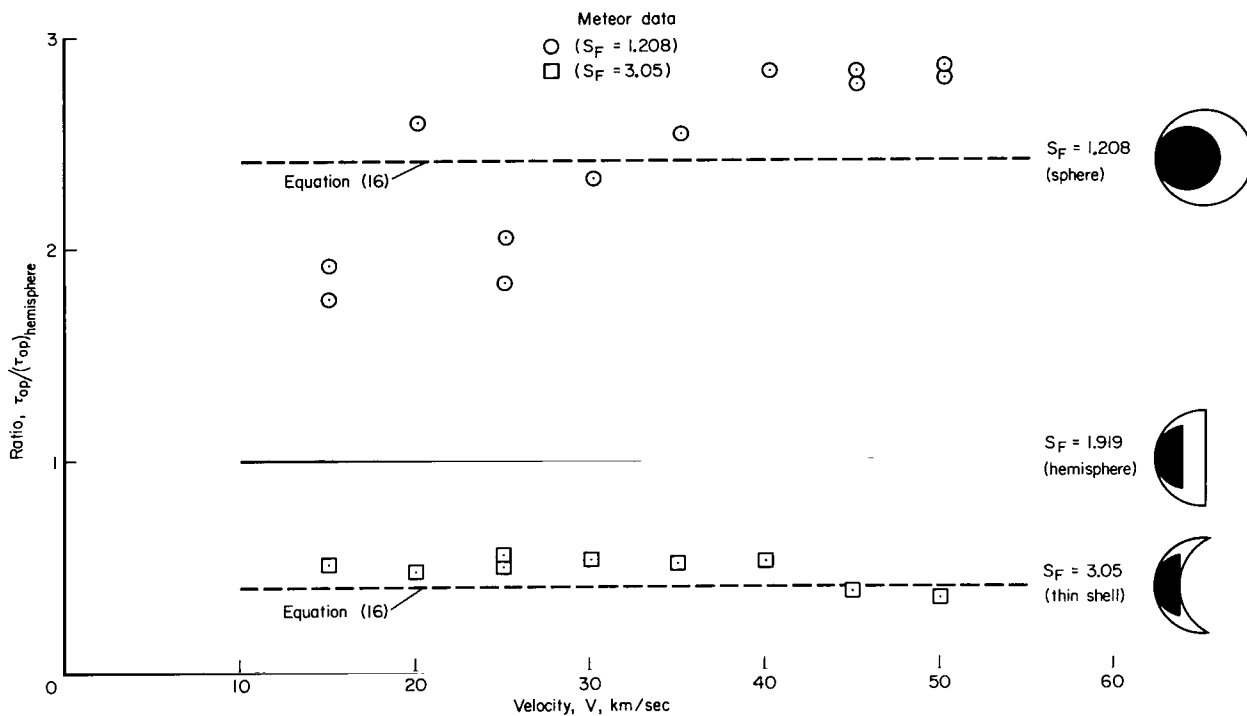

Figure 11.- Effect on luminous efficiency factor of changes in meteoroid shape factor.
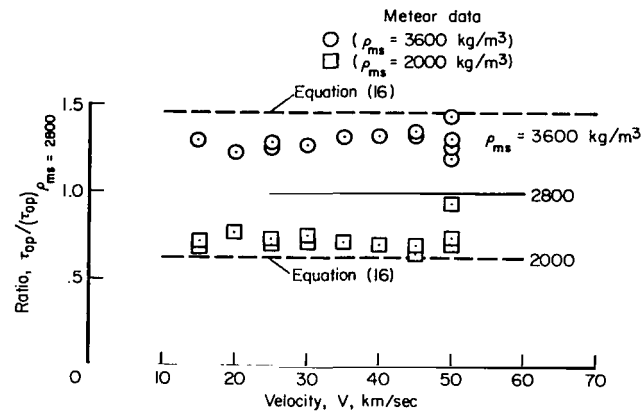
Figure 12.- Effect on luminous efficiency factor of changes in solid meteoroid density.
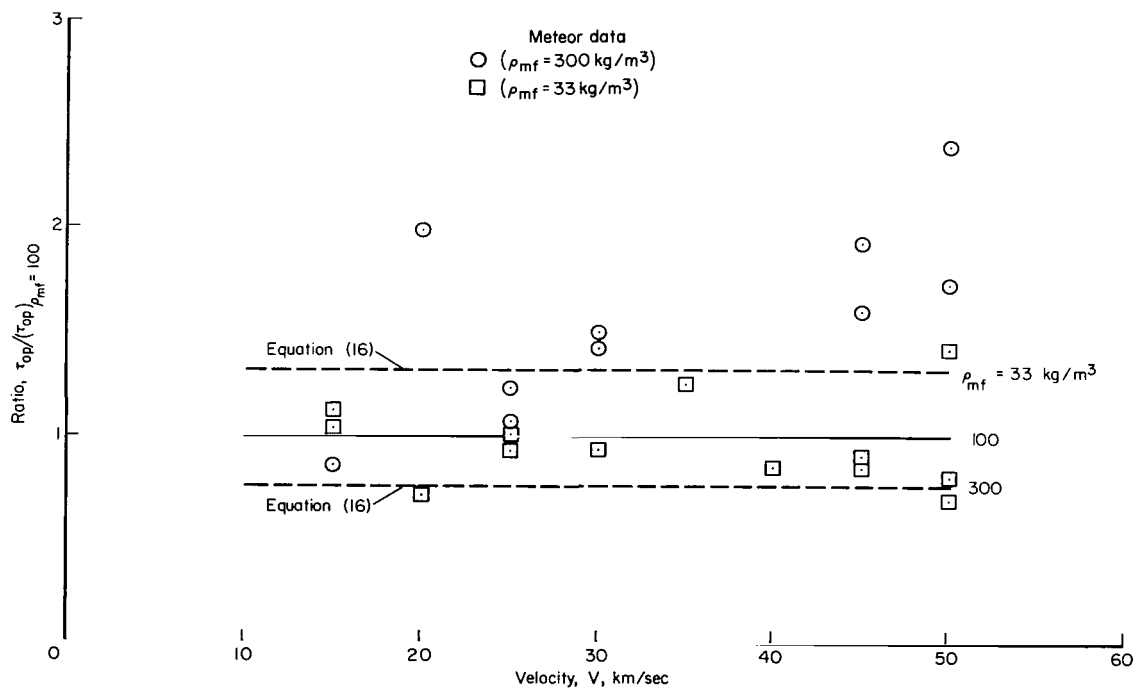

Figure 13.- Effect on luminous efficiency factor of changes in assumed froth density.
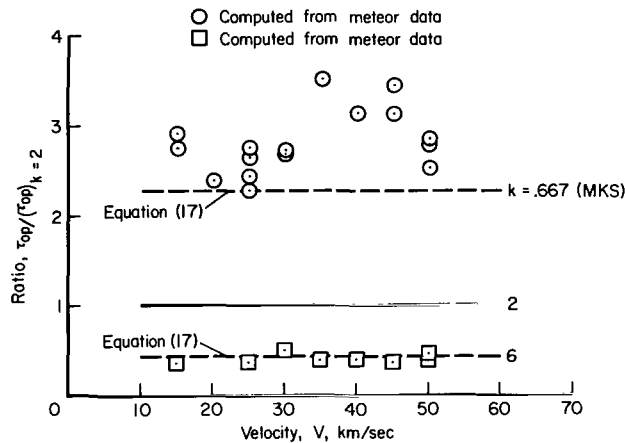
Figure 14.- Effect on luminous efficiency
    factor of changes in thermal
    conductivity.

has been derived. In figure 14 results from machine calculations are compared with the predictions of equation (17) for changes by a factor of 3 in the assigned value of the thermal conductivity k. Since the quantities C_F, k, and C_μ appear only in the combination above in the ablation model equations, figure 14 also indicates the validity of the approximation with respect to variations in their assigned values. The tangential force coefficient C_F depends on computed quantities such as the meteoroid nose radius as well as the air density and meteor velocity. Although C_F is not an assigned parameter, equation (17) indicates the effect on τ_{op} to be expected when C_F is modified by a constant factor due to the reassignment of a parameter such as the constant C in equation (C3).

The equilibrium vapor pressure p_v likewise is not an assigned parameter. However, equation (17) indicates the effect on τ_{op} that would result from a change in the level of the computed vapor pressure due to reassignment of a parameter in the equilibrium vapor pressure law (eq. (C11)). Figure 15 shows a comparison of the prediction with results from machine calculations for a few individual meteors. It is seen that changing the level of the equilibrium vapor pressure law by a factor of 10 changes the computed values of τ_{op} by a factor of about 2.5.
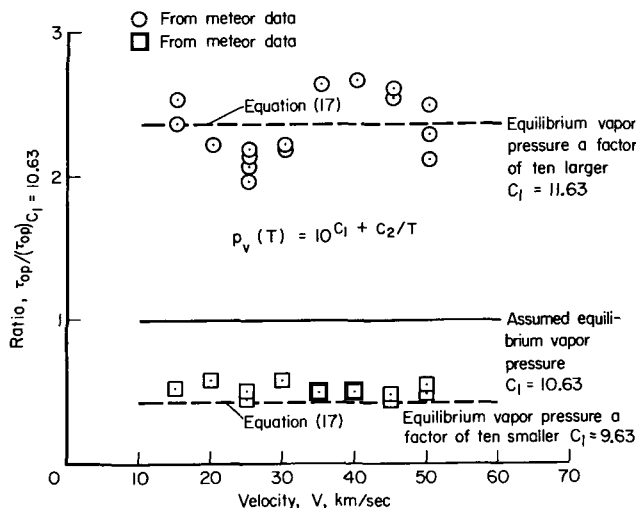

Figure 15.- Effect on luminous efficiency
    factor of changes in level of equilibrium
    vapor pressure.

The quantity ζ_f in equation (17) is the heat per unit mass required to heat and melt the solid meteoroid core; T_f is the temperature of fusion. It has been determined from machine calculations that the effects on τ_{op} of changing the assigned values of these parameters indicated by equation (17) are realistic.

From information given in appendix C, it is found that at a typical temperature of $2400°$ K, ordinary chondrites have a viscosity greater than that of carbonaceous chondrites by a factor of 3.4 and a smaller equilibrium vapor pressure by a factor of 3.6. According to equation (17) the net effect of these

26

two differences is an increase in the predicted values of τ_{op} by a factor of about 1.5. A somewhat smaller effect was found in the machine calculations.

Additional information on the effects of changes in the assigned parameters is given in appendix D. Although the level of the values of τ_{op} in figure 3 may be in error, no simple reassignment of the parameters has been found that would remove the velocity dependence.

Effect of Froth Ablation in Wake

The possibility that the mass determined from the luminosity equation may differ from the dynamic mass has long been recognized. In reference 7, it is observed that if, as a result of aerodynamic forces or thermal stress, material is jettisoned from the body in the solid state or if it flows off the body in the liquid state, there will be a time lag before the debris vaporizes in the wake. The luminosity results from collisions of air and vapor molecules and hence does not appear until the material from the body vaporizes. If a large fraction of the mass is ablated in the solid or liquid form and if the debris follows the parent meteoroid closely enough, the major effect may be simply a lag in the luminous intensity relative to the time of ablation from the parent meteoroid. The mass determined from the luminosity equation would then correspond to the dynamic mass at an earlier time. We shall investigate the consequences of such a mechanism on the computed values of the luminous efficiency factor.

The luminosity equation in the usual form with lag effects neglected can be written

$$m = 2 \int_t^\infty \frac{I_p}{\tau_{op} V^3} \, dt \tag{18}$$

In the development described in the analysis section, this equation is used to determine τ_{op}, the mass and mean meteoroid density being determined from the dynamic and ablation equations. Therefore, if equation (18) is modified, the mass and density computed along a trajectory will not be affected. It is convenient to retain the definition of τ_{op} afforded by equation (18) while defining a corrected luminous efficiency factor τ_{opc} by the relation

$$m = 2(1 - B) \int_t^\infty \frac{I_p}{\tau_{opc} V^3} \, dt + 2B \int_{t+\theta}^\infty \frac{I_p}{\tau_{opc} V^3} \, dt \tag{19}$$

The quantity B is a number between 0 and 1 representing the fraction of the mass ablated as froth, which is vaporized in a time θ after ejection from the parent meteoroid. The fraction $(1 - B)$ of the mass is assumed to be vaporized in a time small compared to θ. It is assumed that a single value of θ and a single value of B in place of an integral over all possible delay times can approximate the effect of the delayed vaporization. If so, τ_{opc} defined by equation (19) may more closely represent the efficiency of

27

converting the kinetic energy of the vapor molecules to photographable light and may be less variable than τ_{op}.

From equations (18) and (19) the mass before entry into the atmosphere is found to be

$$m_{-\infty} = 2 \int_{-\infty}^{\infty} \frac{I_p}{\tau_{op} V^3} \, dt = 2 \int_{-\infty}^{\infty} \frac{I_p}{\tau_{opc} V^3} \, dt$$

If τ_{opc} is less variable than τ_{op}, its use in the relation

$$m_{-\infty} = \frac{2}{\tau_{opc}} \int_{-\infty}^{\infty} \frac{I_p}{V^3} \, dt$$

to determine the meteoroid flux in space is preferable to use of τ_{op} in the same equation. Determinations of τ_{opc} from meteor data may also show less scatter than τ_{op} if part of the variability of τ_{op} is due to an intensity lag. It will be shown that for the 40 meteors analyzed in this report the scatter in τ_{opc} is less than that in τ_{op}.

In appendix E an approximate relationship between τ_{opc} and τ_{op} is derived in the form

$$\tau_{opc} = \tau_{op} \left(1 + B\theta \, \frac{\dot{m}}{m} \right) \tag{20}$$

Since $\dot{m}/m = d\ln(m)/dt$ and τ_{op} are computed along the trajectories of individual meteors in the machine program described in the analysis section, this expression can be used to compute values of τ_{opc} if the product $B\theta$ can be evaluated. We shall first estimate $B\theta$ from a consideration of the behavior of froth particles in the wake and later describe a method for deducing the value from the meteor data.

From the calculations for individual meteors previously discussed, it is found that most of the material ablated from the front face of the solid inner core is removed by flowing to cooler regions rather than by vaporization. This behavior is discussed further in appendix C. The mode of ablation of the froth produced from this flow is not determined by the ablation model described in the analysis section. However, since the froth would be in a cooler region than the front face of the solid core, it can be assumed that most of the froth is ablated in the solid or liquid form rather than by evaporation while attached to the parent meteoroid. For that reason we assume that the quantity B in equations (19) and (20) is approximately equal to 1.

The solidified chunks of froth in the wake would also be expected to ablate by liquid runoff with the drops subsequently breaking up as a result of aerodynamic pressure. When the melted particles produced in this process are small enough to avoid disruption by virtue of surface tension, the subsequent reduction in mass can occur only by vaporization. When the heat sink represented by a progressively exposed cooler interior is absent, the surface

temperature is elevated and rapid vaporization occurs. Our calculations indicate that most of the meteoroid material reaches the vaporized state by this chain of events rather than by direct vaporization from the parent meteoroid (see appendix C).

An approximate expression for the time required for a solid or liquid particle to ablate most of its mass is derived in appendix E in the form

$$\theta = \frac{6\zeta \rho_{mf}^{2/3} m_{fo}^{1/3}}{S_F C_H \rho V^3} \tag{21}$$

where

ζ specific heat of ablation

ρ_{mf} particle density

m_{fo} initial mass

S_F shape factor

C_H heat-transfer coefficient

ρV^2 impact pressure

V particle velocity

All quantities in this expression except the initial mass m_{fo} can be readily estimated. We are concerned with a condition that Öpik (ref. 3) called an abnormal environment in which the particles involved are injected by ablation from a larger body at an altitude lower than they would attain if injected directly from outside the atmosphere. The impact pressure and velocity do not change appreciably during ablation under this condition. The values $\rho V^2 = 3400$ N/m^2 and $V = 2\times10^4$ m/sec corresponding to an early part of the trajectory of meteor 4464 of reference 5 will be used to estimate θ.

We shall first consider the liquid drops held together by surface tension. From a formula in reference 3 it is shown in appendix E that for the above conditions the radius of such particles, considered to be spheres, is

$$r_l = 5.1\times10^{-4} \text{ meter}$$

With the froth density $\rho_{mf} = 100$ kg/m^3, the corresponding mass is

$$m_l = 5.5\times10^{-8} \text{ kg}$$

Substituting this value for m_{fo} and $\zeta = 8.51\times10^6$, $\rho_{mf} = 100$, $C_H = 1$, $\rho V^3 = 6.8\times10^7$, $S_F = 1.208$ in equation (21) yields

$$\theta_l = 0.051 \text{ sec}$$

as the time required to vaporize such liquid drops.

The initial mass of solidified froth particles can be estimated if it is assumed that the sloughing of such particles is observable as fluctuations in the light curve. From light curves in reference 20 and the ablation rate of meteor 4464, a value of

$$m_{fo} = 3 \times 10^{-5} \text{ kg}$$

has been arrived at (appendix E). The radius of a spherical particle of this mass and density $\rho_{mf} = 100 \text{ kg/m}^3$ is

$$r_f = 4.2 \times 10^{-3} \text{ meter}$$

Since liquid ablation rather than vaporization would occur, the specific heat of ablation is taken to be $\zeta = 1.884 \times 10^6$ (ζ_f from table I). With other constants evaluated as before, the resulting lag time from equation (21) is

$$\theta_f = 0.092 \text{ sec}$$

Since the light is not produced until the ablated liquid drops vaporize, the total lag time is

$$\theta = \theta_f + \theta_l = 0.143 \text{ sec}$$

The froth particles are smaller and less dense than the parent meteoroid. They would therefore lag behind and produce most of the light some distance back in the wake. In appendix E an expression for the lag distance is derived in the form

$$\Delta L = \frac{3}{2} \frac{C_D \zeta}{C_H V} \theta \tag{22}$$

The displacements of the liquid drops and froth particles according to this relation with $C_D = 2$, $C_H = 1$, $V = 2 \times 10^4$ meters are

$$\Delta L_l = 0.065 \text{ km (liquid drop)}$$
$$\Delta L_f = 0.026 \text{ km (froth particle)}$$

The total displacement of the region of light production from the parent meteoroid is approximately the sum of these

$$\Delta L = 0.091 \text{ km} \quad \text{(total)}$$

For comparison, the distance covered by a typical meteor between camera shutter breaks is 0.3 km, which is 3 to 10 times larger than the above predicted lag distances.

It is interesting to determine whether there is evidence in the meteor data of an intensity lag time of the order of 0.1 second as predicted in the foregoing discussion. Toward that end, equation (20) can be rearranged in the form

$$\frac{1}{\tau_{op}} = \frac{1}{\tau_{opc}} + \frac{B\theta}{\tau_{opc}} \frac{\dot{m}}{m} \tag{23}$$

The quantities τ_{op} and $\dot{m}/m$ are computed at each trajectory point in the method described in the analysis section. If τ_{opc} and $B\theta/\tau_{opc}$ are assumed to be constant along the trajectory, the computed values of τ_{op} and $\dot{m}/m$ at

Figure 16.- Comparison of intensity lag time from meteor data with estimates (B = 1).

two trajectory points can be used in equation (23) to solve simultaneously for τ_{opc} and $B\theta/\tau_{opc}$. By this means values of $B\theta$ as well as τ_{opc} can be computed from the meteor data. Figure 16 shows values of $B\theta$ thus determined for points on the trajectories of 15 meteors. The computed delay times are plotted versus $10^8/\rho V^3$ to check the dependence on this variable indicated by equation (21). A majority of the points fall reasonably close to the estimated value $\theta = 0.143$ sec arrived at in the preceding discussion. (The estimated value of B is 1.0.)

In appendix E approximate formulas for the delay time as a function of $10^8/\rho V^3$ are derived to obtain

$$\theta_f = 0.063 \times 10^8/\rho V^3 \tag{24}$$

This is the time required to liquefy a froth particle of initial mass $m_{fo} = 3 \times 10^{-5}$ kg (shown as a dashed line in fig. 16). The time required to vaporize liquid drops is approximately (appendix E)

$$\theta_l = 0.0235(10^8/\rho V^3)^2 \tag{25}$$

shown as a broken line in figure 16. The total time required to liquefy the froth particles and vaporize the resulting drops is approximately $\theta_f + \theta_l$ shown as a full line curve in figure 16. Since the initial mass m_{fo} may vary considerably from the assumed value of 3×10^{-5} kg, the comparison of the computed points with the full line curve is satisfactory except for several low points. The low values of $B\theta$ could be explained by an unusually high volatility of the meteroid material such that B is small compared to 1 for these meteors. In that case, vaporization may dominate over liquid runoff for the froth particles. The tendency of values of $B\theta$ computed from the meteor data to lie above the full line curve at small values of $10^8/\rho V^3$ may be due to the presence of larger froth particles or a greater froth density than assumed, or a combination of both. Since figure 16 shows that $B\theta$ varies from meteor to meteor, it is considered preferable to determine its value for each meteor from the data for purposes of evaluating τ_{opc} (rather than utilizing a single value of $B\theta$ for all meteors).

31

As previously mentioned, our machine program computes values of τ_{op} and $\dot{m}$ only at interior points on the trajectory of each meteor. Since calculations at two or more trajectory points are required to evaluate τ_{opc} and $B\theta$ from equation (23), such evaluation can be carried out only for meteors with data given at 4 or more trajectory points in reference 5. For this reason, τ_{opc} can be computed for only 15 of the 40 meteors listed in table II (those marked with the letter a). The statistical procedure previously discussed has been used to determine the dependence of τ_{opc} on velocity. When τ_{opc} could not be computed, it was set equal to τ_{op}. The results are shown in figure 17. Comparison with figure 3 indicates that the scatter in computed values of τ_{opc} is less than the scatter for τ_{op}, although the velocity dependence of the two is similar. There is a small amount of flattening of the velocity dependence at high velocity and a general lowering of values at all velocities.
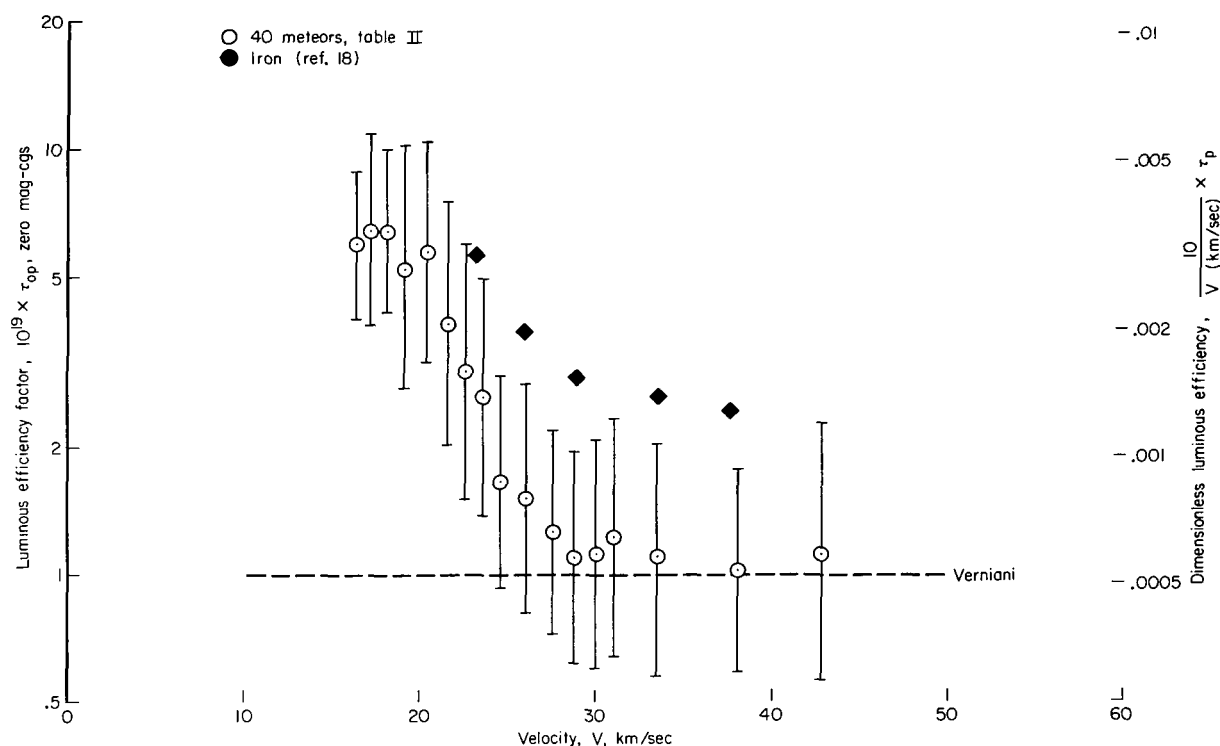

Figure 17.- Luminous efficiency factor with intensity lag correction.

The results for iron from laboratory tests (ref. 18) are also shown in figure 17. The prediction of reference 8 that the luminous efficiency of stone should be less than that of iron by a factor of about 6.5 is more nearly borne out by these results than the uncorrected values shown in figure 3. The remaining discrepancy may be due to a failure of the assumption that the photoelectrically measured luminous efficiency of the tests is equal to the photographic luminous efficiency.

In reference 6 it is noted that calculations of τ_{op} based on an assumed constant density show an apparent increase of τ_{op} along the

32

trajectory for many individual meteors. The effect is ascribed to progressive fragmentation of the virgin meteoroid material. Verniani concludes that, consequently, only the values of τ_{op} from the early parts of the trajectories are reliable. Increases in τ_{op} along the trajectory also result from the present method for many individual meteors. In contrast, the values of τ_{opc} are nearly constant along the trajectories in all cases. Consequently, apparent increases of τ_{op} in references 5 and 6 may be due, in part, to the intensity lag effect. Both decreases and increases of mean meteoroid density along the trajectories are noted from the present method. When decreases in mean density occur, the evaluation of τ_{op} by the method of reference 6 (substitution of a constant value of ρ_m in the ratio τ_{op}/ρ_m^2) would also lead to apparent increases of τ_{op}.

CONCLUDING REMARKS

An ablation model for solid stone meteoroids allowing for a decrease in mean density due to frothing has been used to analyze the data of 40 meteors. Material properties appropriate for carbonaceous chondrites were assigned. The photographic magnitudes of the sample ranged from +1.8 to -3.6. The pre-entry masses computed were between 8×10^{-5} and 3.3×10^{-3} kg, corresponding to radii between 1.9×10^{-3} and 6.5×10^{-3} meter for solid stone spheres. The computed mean densities during atmospheric flight ranged from 300 to 1000 kg/m^3, corresponding to flanges of froth as thick as 7×10^{-3} meter.

The luminous efficiency factor was computed along the trajectory of each meteor and averaged over several meteors in small velocity intervals. The resulting averages agreed with the constant value recommended by Verniani at velocities above 35 km/sec. For velocities below 25 km/sec, τ_{op} was found to rise to about six times Verniani's value.

The effect of a delay in light production resulting from the time required to vaporize chunks of froth in the wake has been investigated. The scatter and the level of computed values of the luminous efficiency factor were reduced slightly by correcting for this delay. The effect can account, in part, for apparent increases of τ_{op} along the trajectories previously attributed to fragmentation. Such increases can also result from the assumption of a constant mean density in cases where the computed mean density decreases due to accumulation of froth. It was found that the data of the 40 meteors analyzed can be explained on the basis of originally solid meteoroids that do not fragment except by sloughing froth produced during the flight.

The properties such as viscosity and equilibrium vapor pressure assigned were chosen to correspond to carbonaceous chondrites. The density of the solid inner core was assumed to be 2800 kg/m^3 and the density of the froth produced during flight was taken to be 100 kg/m^3. An investigation of the effect of changes in the assigned material properties was made. Uncertainties in the properties could alter the level of the computed luminous efficiency factor but not its velocity dependence. Assignment of properties appropriate for ordinary chondrites would not affect the results significantly except for an increase in the predicted stagnation-point surface temperatures. However,

many of the above conclusions would appear to break down if a froth density more than twice the assumed value of 100 kg/m^3 were assigned.

Ames Research Center
National Aeronautics and Space Administration
Moffett Field, Calif., 94035, June 5, 1968
129-01-02-09-00-21

APPENDIX A

DISCUSSION OF ASSUMPTIONS

In addition to the assumptions listed in the analysis section, specific values must be assigned to geometric parameters and constants in the material property laws to carry out an analysis of meteor data. For example, the first assumption can be stated in the form

$$r_n/r = A_{rn} \tag{A1}$$

For most of the calculations, $A_{rn} = 1$ has been used corresponding to a hemispherical front face. However, the effect on the results of changing the ratio to a larger value corresponding to a blunter shape has been investigated.

The second assumption can be expressed as

$$r_s/r = A_{rs}(Q_s/Q)^{1/3} \tag{A2}$$

where A_{rs} is a constant, Q_s is the volume of the solid core, and Q, the total meteoroid volume. The origin and meaning of this relation requires further explanation. Such a rule would apply, for example, if the solid and total volumes were both spheres or hemispheres. Equation (A2) was originally derived for the case of a hemispherical overall shape and a cylindrical solid volume with the length of the cylinder equal to its radius. In the limit of very small r_s/r it can be shown that $A_{rs} = (2/3)^{1/3}$ for that case. This is the value used in the calculations, but the effect on the results of changes in the value of A_{rs} has been investigated. When there is no froth, both r_s/r and Q_s/Q should equal 1, whereas the above value of A_{rs} leads to $r_s/r = 0.874$ at $Q_s/Q = 1$. This 13-percent discrepancy can be used as a basis for judging the error that might arise from the use of assumption 2.

The third assumption is imposed largely for reasons of mathematical expediency and leads to simplification in the analysis of the viscous flow of the thin layer of melted material covering the solid. The presence of meteoroid rotation or oscillation about an axis not alined with the flight direction is denied by this assumption. Such motion might be expected for about one-third of a random sample of meteoroids; however, the amount of scatter in the results due to this assumption is unknown.

The fourth assumption is a statement of the modes of ablation of the solid core that are considered in the present investigation. The last assumption, regarding the composition of the meteoroid, supplies necessary input for the calculations. Most of the results are based on material properties appropriate for carbonaceous chondrites. However, the effect on the calculations of variations in properties has been investigated. It has been found that the values of luminous efficiency factor and meteoroid mean density computed are essentially unchanged when properties appropriate for ordinary chondrites are assumed, although higher surface temperatures result.

The implications of the geometrical assumptions should perhaps be further illustrated. For most of the meteor data to which our ablation model has been applied, the value of the computed ratio of radii r_s/r lies between 0.3 and 0.8. It is of interest to determine the changes in shape that correspond to variations of this ratio as well as changes in the shape factor S_F defined in equation (4). For that purpose it is expedient to make additional geometric assumptions. However, it is worth noting that these additional assumptions are made only for purposes of illustration and are not necessary for application of the ablation model to meteor data.

Since the frontal area is assumed to be circular, equation (4) can be rearranged in the form
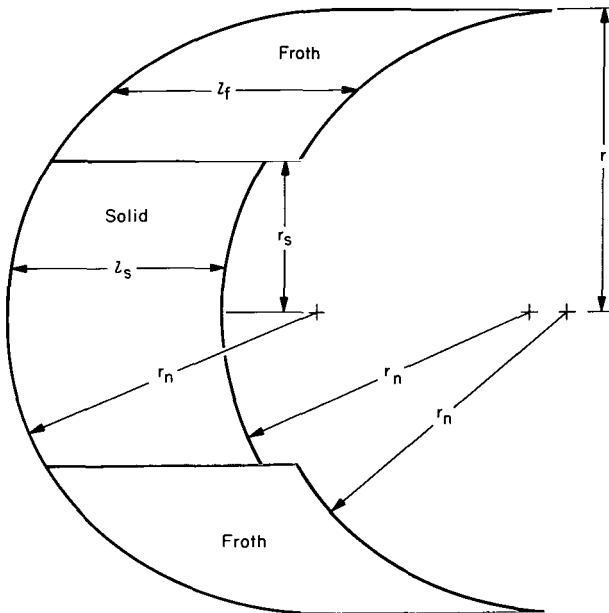
$$Q = \left(\frac{A}{S_F}\right)^{3/2}$$

or

$$Q = \frac{2}{3}\pi r^3 \left(\frac{S_{Fh}}{S_F}\right)^{3/2} \tag{A3}$$

where S_{Fh} is the shape factor for a hemisphere

$$S_{Fh} = \left(\frac{9\pi}{4}\right)^{1/3}$$

Figure 18.- Sketch of circular cylinders with spherical ends used in alternative interpretation of model geometrical relations.

The construction of shapes corresponding to various shape factors and ratios of radii r_s/r is greatly simplified with the assumptions of axial symmetry and spherical ends on the solid and froth cylinders as illustrated in figure 18. In that case the volume of the solid can be written

$$Q_s = \pi r_s^2 l_s$$

Combining this with equation (A3) and rearranging yields

$$\frac{l_s}{r} = \frac{2}{3}\left(\frac{S_{Fh}}{S_F}\right)^{3/2} \frac{Q_s/Q}{(r_s/r)^2} \tag{A4}$$

Similarly, the total volume is given by
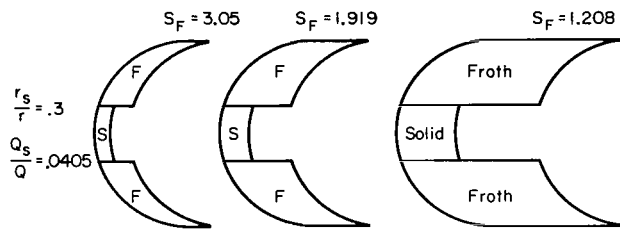
$$Q = \pi r^2 l_f - \pi r_s^2 (l_f - l_s)$$

36

Combination with equation (A3) and substitution of equation (A4) leads to

$$\frac{l_f}{r} = \frac{2}{3} \frac{\left(\frac{S_{Fh}}{S_F}\right)^{3/2} \left(1 - \frac{Q_S}{Q}\right)}{1 - \left(\frac{r_S}{r}\right)^2} \tag{A5}$$

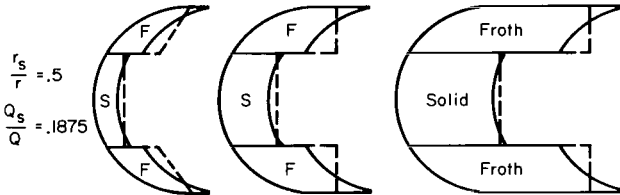The relation arising from assumption 2 given in equation (A2) can be rearranged in the form

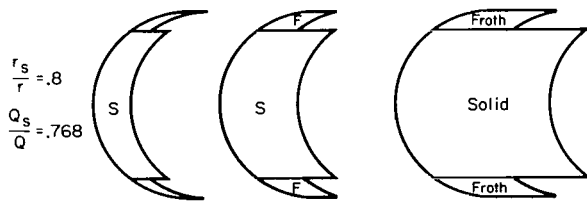$$\frac{Q_S}{Q} = \frac{3}{2} \left(\frac{r_S}{r}\right)^3 \tag{A6}$$

Figure 19.- Sketches of axially symmetric shapes corresponding to various values of shape factor S_F and ratio of solid to total volume Q_S/Q when the front face is a hemisphere.

(The value $A_{rs} = (2/3)^{1/3}$ used in the analysis of meteor data has been inserted.) Substitution of this into equations (A4) and (A5) leads to the relations

$$\frac{l_S}{r} = \left(\frac{S_{Fh}}{S_F}\right)^{3/2} \frac{r_S}{r} \tag{A7}$$

and

$$\frac{l_f}{r} = \frac{2}{3} \left(\frac{S_{Fh}}{S_F}\right)^{3/2} \frac{1 - \frac{3}{2}\left(\frac{r_S}{r}\right)^3}{1 - \left(\frac{r_S}{r}\right)^2} \tag{A8}$$

Figure 19 shows the axially symmetric shapes with spherical ends corresponding to various shape factors S_F and various ratios of solid volume to total volume Q_S/Q. The sketches are generated from equations (A6) to (A8) with the added condition, nose radius r_n equal to base radius r. The column of three sketches on the right corresponds to a shape factor $S_F = 1.208$, which is the same as that of a sphere. The shape factor $S_F = 1.919$ of the middle column is the same as that of a hemisphere, while the value $S_F = 3.05$ of the left column corresponds to what might be termed a thin shell. The three sketches in the top row correspond to a ratio of solid to total volume $Q_S/Q = 0.0405$. The middle and bottom rows correspond to $Q_S/Q = 0.1875$ and 0.768, respectively. Most of the meteors analyzed were found to fall in the range of Q_S/Q covered here. The

37

dotted lines in the middle row of sketches show possible rearrangements of the rear shapes that are allowed within the set of assumptions for the ablation model previously listed. As far as the geometrical assumptions of the model are concerned, even nonaxisymmetric rearrangements of solid and froth volumes are allowed as long as the relative values of the volumes are not changed and the front faces are not altered.

Other allowed shape changes are illustrated by the fact that for the middle column the froth and solid volumes could be packed within a hemisphere without altering the results from analysis of meteor data. Similarly, the volumes in the right column could be fit into spheres without altering results based on a spherical shape factor. The middle column corresponds to the value of shape factor used in most of the calculations in this report, although the effect of a change in shape factor is investigated. The ratio of volumes Q_S/Q is determined at each point on the trajectory of each meteor from the meteor data with the aid of the assumptions of the model.
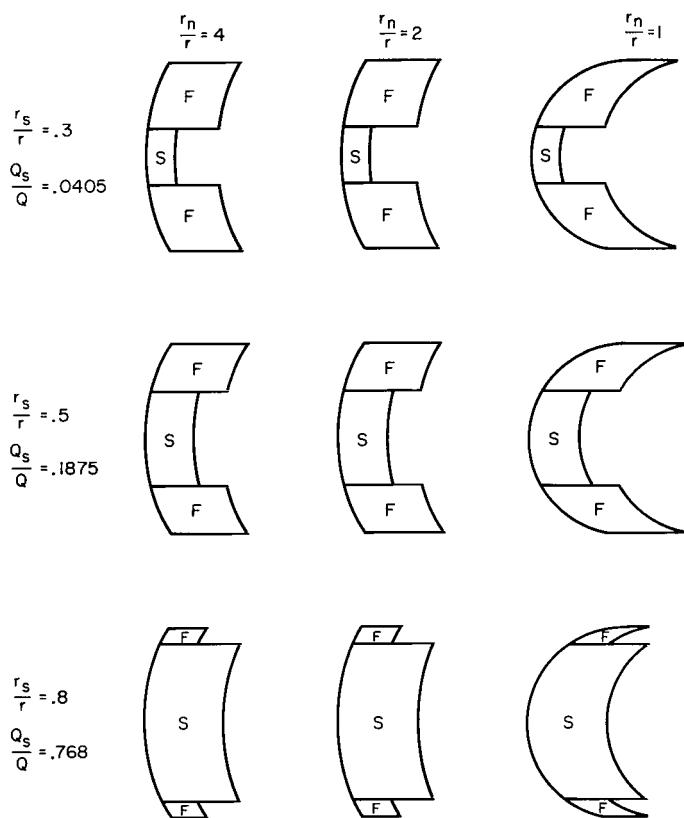

Figure 20.- Axially symmetric shapes corresponding to various degrees of nose bluntness and ratios of solid to total volume ($S_F = 1.919$).

Figure 20 illustrates the effect on the geometry of changes in the ratio of nose radius to the radius of the frontal area r_n/r. Again, rearrangements of the volumes are allowed that preserve the front faces as shown. The right column with the hemispherical front face corresponds to the ratio $r_n/r = 1$ used in most of the calculations, but the effect of varying the ratio is investigated.

Next we shall derive or list the major mathematical relations generated from the ablation model. Auxiliary equations arising from the aerodynamic and material property laws are given in appendixes B and C.

Substituting $Q = m/\rho_m$ into equation (A3) leads to

$$r = \left(\frac{3}{2\pi}\right)^{1/3} \left(\frac{S_F}{S_{Fh}}\right)^{1/2} \left(\frac{m}{\rho_m}\right)^{1/3} \tag{A9}$$

Equation (A1) can be written

$$r_n = A_{rn}r \tag{A10}$$

38

If values of the shape factor S_F and geometric parameter A_{rn} are assigned and the meteoroid mass m and mean density ρ_m are known, the radius of the frontal area r and nose radius r_n can be computed from these equations.

The relation

$$\rho_m Q = \rho_{ms} Q_s + \rho_{mf}(Q - Q_s)$$

expresses the fact that the total meteoroid mass is equal to the sum of the masses of the solid and froth parts. Rearrangement leads to

$$\frac{Q_s}{Q} = \frac{\rho_m - \rho_{mf}}{\rho_{ms} - \rho_{mf}}$$

and substituting this into equation (A2) yields

$$\frac{r_s}{r} = A_{rs} \left(\frac{\rho_m - \rho_{mf}}{\rho_{ms} - \rho_{mf}}\right)^{1/3} \tag{A11}$$

If values of the froth density ρ_{mf}, solid density ρ_{ms}, and geometric parameter A_{rs} are assigned, the radius r_s of the frontal area of the solid can be computed when r and ρ_m are known.

The formula

$$\frac{m}{\rho_m} = \frac{m_s}{\rho_{ms}} + \frac{m - m_s}{\rho_{mf}}$$

arises from the equality of the total meteoroid volume to the sum of the volumes of the solid and froth parts. Differentiation and rearrangement leads to the expression

$$\dot{m}_s = \frac{\rho_{ms}}{\rho_m} \left(\frac{\rho_m - \rho_{mf}}{\rho_{ms} - \rho_{mf}}\right) \dot{m} + \frac{m \rho_{ms} \rho_{mf}}{(\rho_{ms} - \rho_{mf}) \rho_m^2} \dot{\rho}_m \tag{A12}$$

which relates the rate of melting of the solid mass to values and derivatives of m and ρ_m.

Combining equations (A9) and (A11) with the value $S_{Fn} = (9\pi/4)^{1/3}$ inserted leads to the equation

$$A_s = \pi r_s^2 = A_{rs}^2 S_F \left(\frac{m}{\rho_m}\right)^{2/3} \left(\frac{\rho_m - \rho_{mf}}{\rho_{ms} - \rho_{mf}}\right)^{2/3} \tag{A13}$$

for the frontal area of the solid core. The rate of melting of the solid core per unit area and time is given by

$$\omega_s = -\frac{\dot{m}_s}{A_s} \tag{A14}$$

Substituting equations (A12) and (A13) into this and rearranging leads to equation (7) of the text.

For use in appendix B the relation

$$r_n = A_{rn} \sqrt{\frac{S_F}{\pi}} \left(\frac{m}{\rho_m}\right)^{1/3} \tag{A15}$$

is derived by combination of equations (A9) and (A10) with the value $S_{Fh} = (9\pi/4)^{1/3}$ inserted.

APPENDIX B

VISCOUS FLOW EQUATIONS

The relations governing the viscous flow of the melted material covering the front face of the solid are presented here in a form applicable to analysis of arc-jet tests as well as meteors. The configuration under consideration is shown in figure 2.

Basic Relations

An expression for the conservation of mass with respect to an annular control surface at the shoulder of the solid can be written

$$-\rho_{ms}\dot{y} = \frac{2\rho_{mf}u_c\delta_c}{r_s} g_1(T) + \tilde{\omega}(T) \tag{B1}$$

where

$\dot{y}$ rate of recession of the solid surface at the stagnation point

T surface temperature at the stagnation point

u_c tangential surface velocity of the melt at the control surface

δ_c thickness of the melted layer at the control surface

$g_1(T)$ factor to allow for (1) nonlinearity of the velocity profile at the control surface, (2) nonuniformity of the recession rate, and (3) nonuniformity of the surface temperature

$\tilde{\omega}(T)$ rate of evaporation per unit area

The structure of equation (B1) can be understood if $g_1(T)$ is set equal to 1. Then the left side represents the rate of production of melted material per unit area, considered uniform on the entire front face covering the solid. The first term on the right represents the rate of flow of froth through the annular control surface at the shoulder of the solid divided by the frontal area of the solid, πr_s^2. The last term represents the rate of evaporation per unit area, considered uniform over the frontal area.

A question arises as to whether the mass flow through the control surface (the first term on the right) should be based on the density of the solid ρ_{ms} or the froth density ρ_{mf}. In the arc-jet tests, the condition of the models after the tests indicated the material to be frothed in this region. However, this may be due to the sudden drop in pressure resulting from turning off the airstream at the end of the test. In checking equation (B1) against the arc-jet tests, this uncertainty is not important because the combination $\rho_{mf}\delta_c$ is a measure of mass per unit area which can be determined unambiguously

whether the frothing occurred during or after the test. Also, in application of the equation to meteor data, it will be seen that ρ_{mf} and δ_c are eliminated by combination with the other conservation equations. Therefore, the value of the density assigned for the flow in this region is immaterial as long as the same value is used consistently in the other conservation relations.

The momentum equation at the control surface at the shoulder of the solid can be written

$$\frac{\mu_f(T)u_c g_2}{\delta_c} = \frac{1}{2} C_F \rho V^2 \frac{r_s}{r_n} \tag{B2}$$

where

$\mu_f(T)$ viscosity of the froth evaluated at the stagnation-point temperature

g_2 factor to allow for the nonlinearity of the velocity profile and nonuniformity of the temperature

C_F skin-friction coefficient

The viscosity of the froth is used here to be consistent with the use of the froth density in the previous equation. A value of $g_2 = 1$ would correspond to a linear velocity profile. A value of $C_F = 2$ would correspond to free molecule flow, but departures from this condition occur in the analysis of the meteor data in reference 5. The application of equation (B2) to the results of the arc-jet tests reported in reference 14 led to a prediction of values of viscosity consistent with independent measurements. Additional unpublished measurements beyond those reported in reference 14 were made by Charles Shepard at Ames Research Center for this purpose.

An energy equation can be written for a steady state with the assumption of uniform conditions over the frontal area of the solid in the form

$$-\rho_{ms} \dot{y} \zeta_f g_3 = \frac{k(T - T_f)}{\delta_c} \tag{B3}$$

where

ζ_f heat per unit mass required to heat and melt the virgin material

g_3 factor to allow for correction of nonuniformities and nonlinearities

k thermal conductivity

T_f temperature of fusion

Up to the present, the correction factor g_3 has been set equal to 1 for analysis of meteor data. Equation (B3) predicts surface temperatures in the arc-jet tests ranging up to about 2000° K. The surface temperatures were not measured with sufficient precision to check these predictions accurately. It

has been checked that a steady-state equation of the above type is a reasonable approximation for the visible part of meteor trajectories if the meteoroids involved are stone.

For application to meteor data, equations (B1) to (B3) are combined to eliminate u_c and δ_c in the form

$$\left(\frac{k}{\zeta_f}\right)^2 \frac{\rho_{mf}}{\mu_f(T)} (T - T_f)^2 G = - \frac{(\rho_{ms}\dot{y})^2(\rho_{ms}\dot{y} + \tilde{\omega})r_n}{C_F \rho V^2} \tag{B4}$$

where

$$G = \frac{g_1}{g_2 g_3^2} \tag{B5}$$

Available information on the properties of stone at elevated temperatures applies to the unfrothed liquid state. We have assumed that the thermal conductivity of the froth is approximately the same as that of the liquid because of the conductivity of vapor in the bubbles. The viscosity of the froth is expected to be lower than that of the liquid, and we have assumed

$$\frac{\mu_f(T)}{\rho_{mf}} = \frac{\mu(T)}{\rho_{ms}} \tag{B6}$$

Equation (8) of the analysis section follows from equation (B4) by substitution of equations (A15) and (B6) and the relation

$$\rho_{ms}\dot{y} = -\omega_s \tag{B7}$$

Correction Factor for Nonlinear Velocity Profile

The contribution of the nonlinearity of the velocity profile to the correction factor can be determined by setting

$$u_c \delta_c g_1 = \int_0^{\delta_c} u \, dy \tag{B8}$$

and

$$\frac{u_c \mu_f(T) g_2}{\delta_c} = \mu_f(\tilde{T}) \frac{du}{dy} \tag{B9}$$

where $u(y)$ and $\tilde{T}(y)$ are the fluid velocity and temperature at any point y in the profile. If replacements according to these relations were made in equations (B1) and (B2), they would then be exact with respect to nonlinearity of the profile. By partial integration and rearrangement, equation (B8) can be written

$$u_c \delta_c g_1 = \int_0^{\delta_c} \frac{du}{dy} (\delta_c - y) dy$$

If equation (B9) is substituted into this, the relation

$$\frac{g_1}{g_2} = \frac{1}{\delta_c^2} \int_0^{\delta_c} \frac{\mu_f(T)}{\mu_f(\tilde{T})} (\delta - y) dy \tag{B10}$$

can be derived.

In accord with reference 21 the viscosity law is taken to be of the form

$$\frac{\mu_f(T)}{\rho_{mf}} = \frac{\mu(T)}{\rho_{ms}} = C_\mu e^{i/T} \tag{B11}$$

The temperature profile is assumed to be linear so that

$$\tilde{T} = T - (T - T_f)\left(1 - \frac{y}{\delta_c}\right) \tag{B12}$$

Substituting the last two relations into equations (B10) and (B5) with $g_3 = 1$ yields

$$G(T) = \int_0^1 \exp\left\{-\frac{i(T - T_f)\eta}{T[T - (T - T_f)\eta]}\right\} \eta\, d\eta \tag{B13}$$

where

$$\eta = 1 - (y/\delta_c)$$

In the machine program, G is evaluated by 10-point Gaussian quadrature with the interval of integration divided into two parts.

Correction to Account for the Effects of a Pressure Gradient and Meteoroid Acceleration

In the present notation, equation (9) of reference 12 can be written

$$\frac{\partial u}{\partial x} = \frac{d\tau_w}{dx} \int_0^\delta \frac{dy}{\mu} + P^{11} \int_0^\delta \frac{y\, dy}{\mu} \tag{B14}$$

where

$$P^{11} = \left(1 - \frac{\rho_{ms} r_n C_D A}{4m}\right) \frac{2\rho V^2}{r_n^2} \tag{B15}$$

The first term in P^{11} is associated with the augmentation of the viscous flow due to a pressure gradient and the second term provides an estimate of the reduction in mass removal rate due to the meteoroid acceleration. Strictly, equation (B14) applies only at the stagnation point, but to estimate the effects under investigation we shall apply it up to the control surface at the shoulder of the solid inner core. Integration of equation (B14) from $x = 0$ to the control surface at $x \approx r_s$ yields

$$u_c = \tau_{wc} \int_0^{\delta_c} \frac{dy}{\mu} + r_s P^{11} \int_0^{\delta_c} \frac{y \, dy}{\mu} \tag{B16}$$

Equation (B2) follows from this equation if the second term is neglected, μ is considered constant in the integral over y, and with the substitution

$$\tau_{wc} = \frac{1}{2} C_F \rho V^2 \frac{r_s}{r_n} \tag{B17}$$

The same operation applied to both terms of equation (B16), with m/A replaced by $(2/3)\rho_m r$ in equation (B15), leads to

$$\frac{\mu_f(T) u_c g_2}{\delta_c} = \frac{1}{2} C_F \rho V^2 \frac{r_s}{r_n} \left[1 + \left(1 - \frac{3}{8} C_D \frac{\rho_{ms} r_n}{\rho_m r} \right) \frac{2\delta_c}{C_F r_n} \right] \tag{B18}$$

Comparison of equations (B2) and (B18) shows that the correction under consideration can be imposed if C_F is replaced with

$$C_{F_{eff}} = C_F \left[1 + \left(1 - \frac{3}{8} C_D \frac{\rho_{ms} r_n}{\rho_m r} \right) \frac{2\delta_c}{C_F r_n} \right] \tag{B19}$$

Values of δ_c computed from the meteor data with the aid of equations (B3) and (B7) are less than 10^{-4} meter. Also, $C_F > 0.2$, $\rho_{ms}/\rho_m < 9$, $r_n > 4 \times 10^{-3}$ meter for the meteors analyzed. With these extreme values the correction from the pressure term alone is $2\delta_c/(C_F r_n) < 1/4$. When the acceleration term is included, the correction term is $-19/32$, which is numerically larger. In the latter case the quantity in brackets is $13/32$ rather than 1.0 as it is in the absence of pressure gradient and acceleration effects. In other words,

$$C_{F_{eff}} = \frac{13}{32} C_F \tag{B20}$$

The correction represented by equation (B19) has not been applied in the analyses of meteor data of this report. However, an estimate of the error from omission of the correction can be obtained from equation (17) simplified to

$$\tau_{op} \propto C_F^{-3/4} \tag{B21}$$

Thus a change in C_F by the factor 13/32 indicated by equation (B20) would increase the computed value of τ_{op} by the factor $(13/32)^{-3/4} = 1.965$. Most of the computed values of τ_{op} would not receive so large a correction since this value is extreme. However, some of the scatter in the results may be due to omission of the correction.

Comparison With Another Calculation Method

The overall accuracy of the foregoing approximate procedure has been checked by comparison with results from the more exact methods of reference 12.

This was done by constructing artificial meteor data (values of h, V, $\dot{V}$, and m along a trajectory) using the machine program described in reference 12. The machine program of the present report was then used to analyze that data with ρ_{mf} set equal to ρ_{ms} and other material properties equated. Only one step of the iteration described in the analysis section was performed because the result of the comparison rests on whether the value of R from equation (12) is equal to 1 in the first pass. For the cases considered, the values of R computed differed from 1 by less than 20 percent. This indicates that for a meteor the luminous efficiency computed is expected to be in error by less than 10 percent due to the use of the mathematical approximations described in this and the next appendix. It is to be noted that the approximations lead to a considerable reduction in the machine computing time required to analyze the data of large numbers of meteors. In addition, it is not known whether a more elaborate ablation model leading to the evaluation of the luminous efficiency from meteor data is feasible.

APPENDIX C

AUXILIARY RELATIONS FROM AERODYNAMIC AND PROPERTY LAWS

Aerodynamic Relations

The drag coefficient C_D in equation (6) is evaluated by the formula

$$C_D = 1 + e^{-1.837 \times 10^6 \, \bar{\rho}r} \tag{C1}$$

taken from reference 12. The air density ρ and its ratio to the sea level value $\bar{\rho}$ are evaluated according to reference 11.

The temperature T at the stagnation point is found by iterative solution of the energy balance relation

$$\frac{1}{2} C_H \rho V^3 = \epsilon \sigma T^4 + \zeta_v \omega(T) + C_{ms} \zeta_f \omega_s \tag{C2}$$

where

C_H heat-transfer coefficient

ϵ surface emissivity

ζ_v heat per unit mass required to heat, melt, and vaporize the solid

C_{ms} fraction of solid that vaporizes readily or is explosively spalled as it reaches the surface

$\omega(T)$ rate of vaporization (eq. (C10))

ζ_f heat per unit mass required to heat and melt the solid

ω_s rate of melting of solid core mass per unit area and time (eq. (A14))

The term on the left is the heat input from the airstream. The first term on the right represents the heat loss due to surface radiation and the second term, the heat utilized in vaporization of the refractory part of the material. The last term allows for the presence of a volatile component such as water that will evaporate readily when it reaches the surface and which has a negligible latent heat of vaporization after being heated to the melting point of the solid. A fraction of the remaining refractory material might also be carried off by the boiling action from the volatile components. The calculations of this report are based on the properties of carbonaceous chondrites which contain as much as 20-percent water. However, a majority of such meteorites contain less than 20-percent water and we have adopted a value of $C_{ms} = 0.15$.

The vaporization term containing $\omega(T)$ is dominant in the calculations for the meteors of reference 5. Because of the steep temperature dependence of that term, the temperature computed from equation (C2) is insensitive to the values of all parameters appearing in it except those involved in the functional form of $\omega(T)$ itself. For example, it can be shown that with the parameters assigned in table I an increase in C_H or a decrease in ζ_V by a factor of 2 increases the temperature computed by less than $60°$ K. Changes in the parameter ϵ or C_{ms} in equation (C2) by a factor of 2 would have less effect. For the calculations in this report we have set $\epsilon = 0.6$, $\zeta_V = 8.51 \times 10^6$ (m/sec)^2 and $\zeta_f = 1.884 \times 10^6$ (m/sec)^2. The values of all parameters are listed in table I.

The additional terms $(1 - C_{ms})\zeta_f\omega_s - \zeta_f\omega(T)$ would be required in equation (C2) for computing an average temperature over the entire solid frontal area. This would account for the fraction of the input energy utilized to heat and melt the solid material removed by the viscous flow. The resulting decrease in temperature below that computed from equation (C2) is not evaluated in the present model. However, the effect can be accounted for approximately by setting C_{ms} in equation (C2) equal to an artificially large value. The insensitivity of the results to an increase of C_{ms} by a factor of 2 above the assigned value is considered to be an indication that computation of the temperature drop is not essential.

The heat-transfer coefficient C_H is evaluated by formulas taken from references 7 and 12 as follows:

$$C_{Hcvu} = \frac{CV^{P_v}}{\sqrt{\bar{\rho}} r_n} \left[\sigma_1 + \frac{1 - \sigma_1}{1 + \frac{\alpha V^2}{\zeta_v} \left(\frac{\zeta_v \omega}{\epsilon \sigma T^4 + \zeta_v \omega} \right) \exp(-7.2 \times 10^{-8}/\bar{\rho}r)} \right] \tag{C3}$$

$$C_{Heu} = 41.6 \bar{\rho}^{0.8} \left(\frac{V}{10^4} \right)^{2.05} r_n e^{-7.2 \times 10^{-8}/\bar{\rho}r} \tag{C4}$$

$$C_{Huu} = 0.6 \times 10^{-3} \left(\frac{V}{10^4} \right)^4 e^{-7.2 \times 10^{-8}/\bar{\rho}r} \tag{C5}$$

$$C_{Hu} = C_{Hcvu} + C_{Heu} + C_{Huu} \tag{C6}$$

$$C_H = C_{Hu} e^{-2C_{Hu}} + (1 - e^{-C_{Hu}})^2 \tag{C7}$$

The units in this report are MKS except where noted. Values of the required parameters used in the calculations are listed in table I. The quantity C_{Hcvu} is a convective heat-transfer coefficient that allows for the presence of ablation vapor. It is not necessary to include the radiative heat-transfer coefficients C_{Heu} (equilibrium) and C_{Huu} (nonequilibrium) for the analysis of meteors corresponding to meteoroids below 1 gram in mass. These terms

contribute significantly only in the case of bright meteors. Equation (C7) is a bridging formula applicable in the entire range of continuum, transition, and free molecule flow. This relation, taken from reference 7, compares favorably with a bridging formula derived in reference 12. In the analysis of the super-Schmidt meteor data of reference 5, values of C_H ranging from 0.1 to 1.0 were computed.

The rate of vaporization per unit mass for free molecule flow ω_{FM} is given by the Langmuir equation

$$\omega_{FM} = 0.1383 \frac{\sqrt{M} \, p_V(T)}{\sqrt{T}} \qquad (C8)$$

where

M   molecular weight

$p_V(T)$ equilibrium vapor pressure (eq. (C11))

When governed by diffusion in the presence of a viscous boundary layer, the rate of vaporization can be approximated by

$$\omega_d = \frac{34.4 M C_{Hc} v u p_V(T)}{V\left[1 - \dfrac{p_V(T)}{\rho_o \overline{\rho} V^2}\right]} \qquad (C9)$$

which is a modified form of a relation given in reference 12.

A bridging formula for the general case derived in reference 12 is the relation

$$\frac{1}{\omega} = \frac{1}{\omega_{FM}} + \frac{1}{\omega_d} \qquad (C10)$$

The equilibrium vapor pressure in equations (C8) and (C9) is given by

$$p_V(T) = 10^{c_1 + c_2/T} \qquad (C11)$$

When $p_V(T)$ approaches the Newtonian pressure $\rho_o \overline{\rho} V^2$ in equation (C9), the contribution of the diffusion term in equation (C10) goes to zero. When $p_V(T)$ exceeds $\rho_o \overline{\rho} V^2$, the diffusion term is omitted. For the reasons discussed following equation (C2) the computed temperature is insensitive to the molecular weight assigned. The value adopted is $M = 0.03985$ kg/mole. The most critical link in the evaluation of $\omega(T)$ and the stagnation temperature T is the equilibrium vapor pressure law (eq. (C11)), which is discussed at the end of this appendix.

Allowance is made in equation (C2) for rapid evaporation or explosive spalling of a fraction C_{ms} of the solid material as it reaches the surface. The total rate of evaporation per unit area by this means and by vaporization of the remaining more refractory component is given by

$$\tilde{\omega} = \omega + C_{ms}\omega_s \tag{C12}$$

Since $\tilde{\omega}$ appears in the viscous flow equation (8), the effect of an error in the choice of C_{ms} must be considered again in that connection. However, from the results of an investigation similar to that leading to equations (16) and (17) it can be shown that an increase of C_{ms} by a factor of 2 would lead to an error of less than 20 percent in the computed luminous efficiency factor. This finding depends partly on the choice of other parameters. With the parameters assigned in table I the calculations indicate that for the meteors analyzed the fraction of the solid evaporated is less than 25 percent of that removed by viscous flow.

This finding conflicts with the conclusion reached by Öpik (ref. 3) that solid stone meteoroids would evaporate rather than ablate by viscous flow. The difference arises partly from the added term $1/\omega_d$ in equation (C10) which often leads to a reduction in the evaporation rate below that computed by Öpik based on equation (C8) alone. The viscosity used in our calculations is also an order of magnitude below Öpik's value as indicated in the discussion at the end of this appendix. Further, Öpik computes the surface temperatures that would correspond to ablation by vaporization alone and viscous flow alone. If the latter exceeds the former, he assumes that vaporization will dominate. However, if both ablation processes were considered simultaneously, a surface temperature below either of those computed would apply. A reduction in temperature leads to a much greater decrease in the rate of vaporization than in the ablation due to viscous flow. As a result, we find that efficient vaporization of stone or iron can occur only if the scale is such that ablation by viscous flow is impeded by surface tension.

In reference 12 the skin-friction coefficient for continuum flow is determined by a Reynolds analogy between energy transfer and momentum transfer and is given by

$$C_{Fu} = 2C_{Hcvu}/\sqrt{\rho_{21}} \tag{C13}$$

where ρ_{21} is the density ratio across a normal shock and C_{Hcvu} is the convective heat-transfer coefficient given in equation (C3). For the calculations in this report, we have set $\rho_{21} = 9$. A bridging formula analogous to equation (C7) is

$$C_F = C_{Fu}e^{-C_{Fu}} + 2(1 - e^{-C_{Fu}/2})^2 \tag{C14}$$

This relation yields the correct tangential force coefficient for free molecule flow, $C_F = 2$, when C_{Fu} becomes large.

Viscosity and Vapor Pressure Laws

The assignment of material properties for analysis of meteor data in this report is based on information contained in references 3, 15, 21, and 22 as well as unpublished experimental measurements. The properties of carbonaceous chondrites and ordinary chondrites were considered to be of primary interest. Information on the properties of such material was contributed by
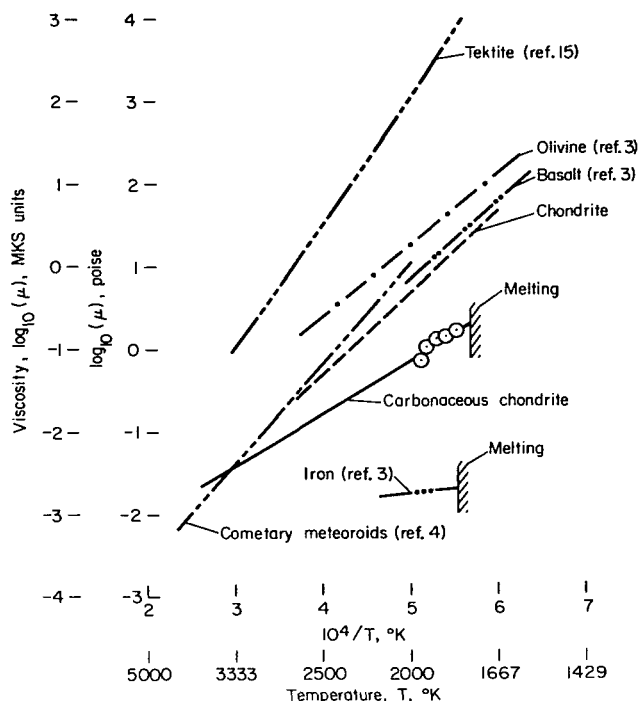
Figure 21.- Viscosity as a function of temperature.

○ Synthetic carbonaceous chrondrite measurements (Zimmerman)
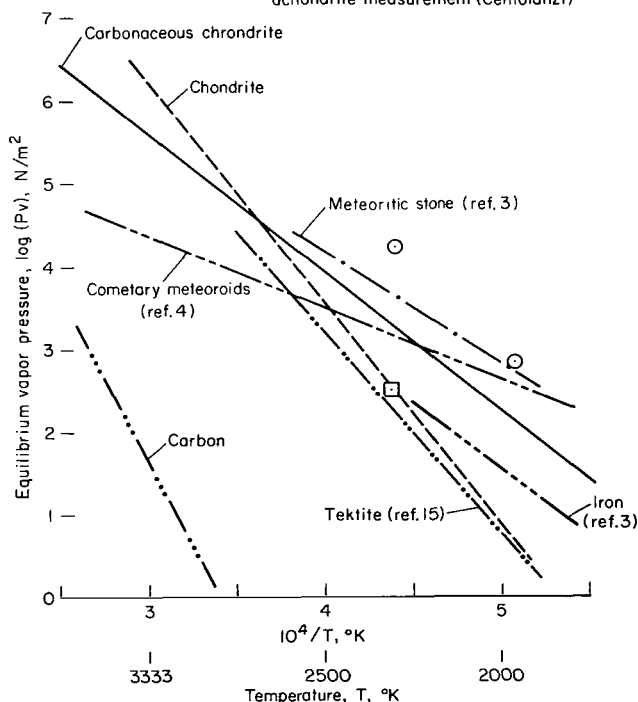□ Norton county Kansas enstatite achondrite measurement (Centolanzi)

Figure 22.- Equilibrium vapor pressure as a function of temperature.

Dean Chapman and Klaus Keil of the Ames Research Center. The vapor pressure of an enstatite achondrite was measured by Frank Centolanzi at Ames Research Center. The vapor pressure of a synthetic carbonaceous chondrite material prepared by Klaus Keil was measured by Norman Zimmerman at Ames. Viscosity, thermal conductivity, and heat capacity were measured by the Corning Glass Company as part of a larger contract monitored by Frank Centolanzi.

Figure 21 shows the viscosity of various stones and iron as a function of temperature. According to reference 21, log μ is expected to depend linearly on the inverse of the temperature. The full line indicates the viscosity considered to be representative of carbonaceous chondrite. The small circles are experimental data points. A slope intermediate between that of iron and basalt was adopted. We have taken the dashed line near Öpik's values for basalt to be representative of ordinary chondrites. The values of the parameters appearing in equation (B11) based on the full line curve with $\rho_{ms} = 2,800$ kg/m^3 are $C_\mu = 1.525 \times 10^{-8}$ (MKS) and $i = 14,800°$ K for carbonaceous chondrites. From the dashed line $C_\mu = 1.655 \times 10^{-9}$ and $i = 23,030°$ K for ordinary chondrites. The calculations in this report are based on the properties of carbonaceous chondrites (the full line in figure 21). The effect on the results of possible errors from this choice is discussed in the Results and Discussion section.

Figure 22 shows the equilibrium vapor pressure p_v as a function of temperature for several materials. From thermodynamic considerations log p_v is

expected to depend linearly on the inverse of temperature with the negative slope proportional to the latent heat of vaporization (ref. 23). The circles represent unpublished experimental measurements of the vapor pressure of a synthetic carbonaceous chondrite material. Because of the volatility of some components of the mixture, it was considered advisable to allow for rapid evaporation of a fraction of the material and adopt a lower vapor pressure for the remaining more refractory part. The vapor pressure for carbonaceous chondrites was therefore taken to be intermediate between the measurements and the values for ordinary chondrites as shown by the full line. The vapor pressure adopted for ordinary chondrites is shown by the dashed line. The square data point represents a measurement of a sample from an enstatite achondrite with the slope established by comparison with measurements of similar terrestrial materials not shown on the figure. The broken line labeled cometary meteoroids is the vapor pressure used in reference 4 to compute the luminous efficiency from meteor data. The small slope was used to bring results from bright meteor data into agreement with the super-Schmidt data. However, the resulting low meteoroid mean densities for bright meteors are not now considered realistic for such large objects on the basis of the arc-jet tests described in reference 14.

The values of the parameters c_1 and c_2 appearing in equation (C11) corresponding to the full line in figure 22 are $c_1 = 10.63$ (MKS) and $c_2 = -16,750°$ K for carbonaceous chondrites. For ordinary chondrites as represented by the dashed line, $c_1 = 14.215$ (MKS) and $c_2 = -26,700°$ K. The calculations in this report are based on the properties of carbonaceous chondrites, but the effect on the results of modifications of the equilibrium vapor pressure law is considered in the Results and Discussion section and appendix D.

APPENDIX D

APPROXIMATE RELATIONS SHOWING EFFECTS OF CHANGES IN ASSIGNED PARAMETERS

The sensitivity of the calculations to modifications of the assigned parameters, considered in the Results and Discussion section, has been determined by approximation of equations (3), (7), and (8). For that purpose, it has been found advantageous to utilize approximate proportionality relations in the place of complicated expressions:

If the ratio τ_{op1}/τ_{op} in equation (3) is considered constant along the trajectory for each meteor, equation (3) can be approximated by

$$m \cong \frac{\tau_{op1}}{\tau_{op}} m_1 \qquad (D1)$$

Differentiation of equation (3) with respect to time yields

$$\dot{m} = \frac{\tau_{op1}}{\tau_{op}} \dot{m}_1 \qquad (D2)$$

Equations (D2) and (D1) lead to

$$\dot{m} \cong \frac{\dot{m}_1}{m_1} m \qquad (D3)$$

Let us consider a calculation based on values of the assigned parameters different from those used to compute m. The resulting values of mass m_a along the trajectory of a meteor will differ from the values of m computed with the parameters assigned according to table I. Equation (D3) will still apply, however, in the form

$$\dot{m}_a \cong \frac{\dot{m}_1}{m_1} m_a$$

The values of the ratio $\dot{m}_1/m_1$ are unchanged by the reassignment of parameters since they arise directly from the input quantities $(h, V, \dot{V}, m_1)$ taken from reference 5. Therefore, dividing the last relation by equation (D3) yields

$$\frac{\dot{m}_a}{\dot{m}} \cong \frac{m_a}{m}$$

This can be expressed as the proportionality relation

$$\dot{m} \propto m \qquad (D4)$$

which applies with respect to variations of the assigned parameters. That is, the computed value of $\dot{m}$ on a point of the trajectory of a particular meteor will change by the same fractional amount as the computed value of mass changes due to a reassignment of parameters.

For small variations of ρ_{ms} or ρ_{mf} from their assigned values, the factor

$$y = \frac{\rho_m - \rho_{mf}}{\rho_{ms} - \rho_{mf}}$$

appearing in equation (7) is approximately proportional to a product of powers of ρ_m, ρ_{ms}, and ρ_{mf}

$$\frac{\rho_m - \rho_{mf}}{\rho_{ms} - \rho_{mf}} \cong C\rho_m^a \rho_{ms}^b \rho_{mf}^c$$

where C is a constant. Variations of ρ_m from its computed value must be considered because of the effect of changes in ρ_{ms} or ρ_{mf} in other equations. The operation $\partial \ln(y)/\partial \rho_m$ performed on both sides of the last equation and rearrangement leads to

$$a = \frac{\rho_m}{\rho_m - \rho_{mf}}$$

Evaluating the right side at the typical values $\rho_m = 0.4$ g/cm^3 and $\rho_{mf} = 0.1$ g/cm^3 yields a = 4/3. Similarly, partial logarithmic differentiation with respect to ρ_{ms} and ρ_{mf} with $\rho_{ms} = 2.8$ g/cm^3 leads to b = -28/27 and c = -8/27. Since the initial computed value of ρ_m can differ from 0.4, the exponents b and c have been simplified to -1 and -1/3. Therefore, the following approximate proportionality is arrived at

$$\frac{\rho_m - \rho_{mf}}{\rho_{ms} - \rho_{mf}} \propto \rho_m^{4/3} \rho_{ms}^{-1} \rho_{mf}^{-1/3} \tag{D5}$$

For changes in ρ_m, ρ_{ms}, or ρ_{mf} by a factor of 2 from their initial values, the error in this approximation is less than 20 percent, although each of the quantities on the two sides changes by as much as a factor of 3. Gross inaccuracies arise only when ρ_m approaches ρ_{mf} such that the left side changes by an order of magnitude. Equation (D5) applies with respect to variation of any assigned parameter. The factors ρ_{ms}^{-1} and $\rho_{mf}^{-1/3}$ could be dropped out of the right side of equation (D5) if we wished to consider the effects of variations of other assigned parameters while holding ρ_{ms} and ρ_{mf} fixed. In contrast, the factor $\rho_m^{4/3}$ could not be dropped for any case because ρ_m is a computed quantity rather than an assigned quantity.

From the machine calculations it has been ascertained that the term in equation (7) containing $\dot{\rho}_m$ is ordinarily small compared to the first term containing $\dot{m}$. In that case the approximate proportionality relation

$$\omega_s \propto A_{rs}^{-2} S_F^{-1} \rho_m^{1/9} \rho_{ms}^{2/3} \rho_{mf}^{-1/9} m^{1/3} \tag{D6}$$

can be derived from equation (7) with the aid of equations (D4) and (D5).

Equation (8) leads to the proportionality

$$F \propto A_{rn} S_F^{1/2} m^{1/3} \rho_m^{-1/3} \omega_s^2 (\omega_s - \tilde{\omega}) C_F^{-1} (\rho V^2)^{-1} \tag{D7}$$

where

$$F = \left(\frac{k}{\zeta_f}\right)^2 \frac{\rho_{ms}}{\mu(T)} (T - T_f)^2 G(T) \tag{D8}$$

The factor $(\rho V^2)^{-1}$ need not be retained for variations of the type under consideration since it depends only on the input data (h, V, $\dot{V}$, m_1) and would not be affected by changes in any assigned parameter. Also, $\tilde{\omega}$ is ordinarily small compared to ω_s so that the relation

$$\omega_s^3 \propto A_{rn}^{-1} S_F^{-1/2} m^{-1/3} \rho_m^{1/3} F C_F$$

can be derived from equation (D7).

Substituting equation (D6) into the last equation and rearranging it yields

$$m^{4/3} \rho_{ms}^2 \rho_{mf}^{-1/3} \propto A_{rn}^{-1} A_{rs}^6 C_F F S_F^{5/2}$$

Further rearrangement leads to the relation

$$m \propto A_{rn}^{-3/4} A_{rs}^{9/2} S_F^{15/8} \rho_{ms}^{-3/2} \rho_{mf}^{1/4} C_F^{3/4} F^{3/4} \tag{D9}$$

All quantities appearing in this expression are assigned parameters except m, C_F, and F which are computed, but also depend on additional assigned parameters. However, it can be shown that C_F and F are rarely sensitive to changes in the assigned parameters contained explicitly in equation (D9). Therefore, C_F and F can be dropped from equation (D9) for purposes of considering such variations. The effect of changes in the assigned parameters contained in C_F and F can be considered separately by omitting all factors except C_F and F. In other words, equation (D9) can be factored into the two relations

$$m \propto A_{rn}^{-3/4} A_{rs}^{9/2} S_F^{15/8} \rho_{ms}^{-3/2} \rho_{mf}^{1/4} \tag{D10}$$

and

$$m \propto C_F^{3/4} F^{3/4} \tag{D11}$$

by virtue of an approximate independence of the two factors with respect to the types of variations of assigned parameters under consideration.

The nature of the approximation can be understood by considering a variation of A_{rn}. According to equation (D10), this would change the computed values of m, which would change the radii r_n and r in equation (C3), so that C_{Hcvu} and C_F evaluated by equations (C13) and (C14) would be altered. Therefore, strictly, C_F depends on m and should be retained in equation (D9) which would invalidate equation (D10). However, equation (C3) shows that C_{Hcvu} depends on $m^{1/6}$ (since $r_n \propto m^{1/3}$) if we exclude the few cases where the exponential term causes a stronger coupling. Therefore, an accurate evaluation with C_F included in equation (D10) would differ only slightly from the result obtained by excluding it, except possibly for a few points on

the trajectories of a small number of meteors. The statistical procedure would tend to suppress the effect of the exceptional cases in the computed averages.

The quantity F is defined in equation (D8). For a particular meteor, F depends only on the stagnation-point temperature T and the assigned parameters contained in the material property laws. In other words, F depends on the other computed quantities such as m only through their effect on T. But it can be seen from equation (C2) and the discussion thereafter that this dependence is weak. Therefore, omitting F from equation (D10) is not expected to cause serious error in the consideration of the effects of variations of the assigned parameters A_{rn}, A_{rs}, S_F, ρ_{ms}, and ρ_{mf}. If we wish to consider the effect of variation of only one of the assigned parameters in equation (D10), the others can be omitted from that equation since they are to be held fixed in the variation. For that reason, equation (D11) follows from equation (D9) under the condition that the assigned parameters A_{rn}, A_{rs}, S_F, ρ_{ms}, and ρ_{mf} are to be held fixed.

The derivation of equations (D10) and (D11) is based on the assumption that the stagnation temperature T is approximately independent of variations in the assigned values of geometric parameters. This means that T is assumed to depend only on input quantities and assigned parameters appearing in the aerodynamic and material property laws. That dependence will be considered explicitly so that equation (D11) can be interpreted in terms of variations of the assigned parameters. However, it is worth noting at this point that, by virtue of the approximations employed, the values of mass computed have been found to depend only on the assigned parameters contained in the ablation model. Within the accuracy of the approximations of this appendix, the values of mass do not depend on the luminosity and dynamic equations.

The relation

$$m \propto \tau_{op}^{-1} \tag{D12}$$

follows from equation (D1). Substituting this into equation (D10) leads to equation (16) of the Results and Discussion section. Again, it is worth noting that within the accuracy of the approximations of this appendix neither the mass nor the luminous efficiency factor depends on the dynamic equation. This means that values of the luminous efficiency factor and mass computed by the machine program are expected to be insensitive to errors in the accelerations that may exist in the reduced meteor data used as input. The effect of such errors, if present, would be confined largely to the computed values of mean meteoroid density.

In order to determine the effect on the mass and the luminous efficiency factor of changes of the assigned parameters in the aerodynamic and material property laws, a further analysis of the quantity F defined in equation (D8) is needed. The first step in this procedure is to determine how changing these parameters affects the computed stagnation-point temperature.

The term $\epsilon\sigma T^4$ in equation (C2) is ordinarily small compared to the other terms. If it is omitted, the temperature can be evaluated in two steps:

(1) The vapor pressure p_{vc} is determined by equations (C2) to (C10). The subscript c is intended to indicate that the vapor pressure under consideration is computed from the aerodynamic relations and does not depend on the assignment of parameters in the equilibrium vapor pressure law. (2) The value of p_{vc} from the first step is used to determine the stagnation-point temperature T from equation (C11). For that purpose, equation (C11) can be rearranged in the form

$$c_1 + \frac{c_2}{T} = \log p_{vc}$$

Let us consider the effect on T of variations in c_1 or p_{vc} and let the subscript b refer to the base values corresponding to the assigned values in table I. The relation

$$c_1 + \frac{c_{2b}}{T} = c_{1b} + \frac{c_{2b}}{T_b} + \log \frac{p_{vc}}{p_{vb}}$$

is obtained by combining two equations of the above form and indicates the effect on T of changes in c_1 or p_{vc}. Rearrangement leads to the equation

$$c_{2b} \frac{(T_b - T)}{T_b T} = c_{1b} - c_1 + \log \frac{p_{vc}}{p_{vb}}$$

Since T will not differ greatly from T_b, a typical value of $2,400^O$ K can be used for both T_b and T in the denominator on the left. Upon insertion of the value $c_{2b} = -16,750$ from table I as well, the relation

$$T - T_b \cong 340 \left(c_{1b} - c_1 + \log \frac{p_{vc}}{p_{vb}} \right)$$

can be arrived at.

The last expression indicates that if the equilibrium vapor pressure law (eq. (C11)) is modified so that the level of vapor pressure at a given temperature is higher by a factor of 10 ($c_1 = c_{1b} + 1$), the computed temperatures will all be decreased 340° K. The expression also indicates that if the value of p_{vc} computed from the aerodynamic relations is increased by a factor of 10 the computed temperature will increase 340° K. It can be seen that reasonable reassignments of the parameters in the aerodynamic laws, equations (C2) to (C10), lead to changes in p_{vc} by a factor of order 2 rather than 10. This would change the computed temperatures about 100° K. Changes in p_{vc} due to alterations of other computed quantities such as m or r are ordinarily much less than a factor of 2.

It will be seen that a change of 100° K leads to a modification of about 30 percent in the computed values of the luminous efficiency factor. Therefore, we shall drop the consideration of effects of modifications other than the level of the equilibrium vapor pressure law (the value of c_1) and rewrite the last expression as

$$T - T_b \cong 340 \log \frac{p_{vb}}{p_v} \tag{D13}$$

where $c_{1b} - c$ has been replaced by $\log(p_{vb}/p_v)$ for notational convenience. This relation will be used to evaluate the temperature appearing in the quantity F.

Substituting equation (B11) into (D8) yields

$$F = \left(\frac{k}{\zeta_f}\right)^2 C_\mu^{-1} e^{-i/T} (T - T_f)^2 G(T)$$

The function $G(T)$ defined in equation (B13) can be approximated by

$$G(T) \cong \frac{\left(\dfrac{T}{i}\right)^2}{\left(1 - \dfrac{T_f}{T}\right)^2 + 2\left(\dfrac{T}{i}\right)^2}$$

so that

$$F \cong \left(\frac{k}{\zeta_f}\right)^2 \frac{C_\mu^{-1} e^{-i/T} (T - T_f)^2 \left(\dfrac{T}{i}\right)^2}{\left(1 - \dfrac{T_f}{T}\right)^2 + 2\left(\dfrac{T}{i}\right)^2}$$

The dependence of F on all quantities except i in the above expression can be approximated by

$$F \cong C\left(\frac{k}{\zeta_f}\right)^2 C_\mu^{-1} T_f^b e^{\frac{T-T_b}{T_A}}$$

for small deviations of the assigned parameters or T from their base values. The quantities b and T_A are constants to be evaluated and C is a proportionality constant. If partial derivatives with respect to T_f and T of the logarithms of the last two expressions for F are equated and evaluated at the typical values $T = 2,400^\circ$ K, $T_f = 1,800^\circ$ K, $i = 14,800^\circ$ K, one finds $b = 0.25$ and $T_A = 292^\circ$ K. Substituting these into the last expression for F yields the proportionality relation

$$F \propto \left(\frac{k}{\zeta_f}\right)^2 C_\mu^{-1} T_f^{1/4} e^{\frac{T-T_b}{292}} \tag{D14}$$

Using this expression in equations (D11) and (D12) shows that a change in temperature $T - T_b = 100^\circ$ K leads to less than a 30-percent change in τ_{op}.

Substituting equation (D13) into (D14) replaces the temperature dependent exponential factor with the factor $(p_{vb}/p_v)^{0.505}$. Since the typical value of T used in the derivation is not exact, the exponent 0.505 can be replaced by $1/2$. Also, the base vapor pressure p_{vb} corresponding to the assigned parameters in table I can be dropped from the proportionality relation since it does not depend on any reassigned parameters. The resulting proportionality relation for F is

$$F \propto \left(\frac{k}{\zeta_f}\right)^2 C_\mu^{-1} T_f^{1/4} p_v^{-1/2} \tag{D15}$$

Substituting equation (D15) into (D11) yields

$$m \propto C_F^{3/4} \left(\frac{k}{\zeta_f}\right)^{3/2} C_\mu^{-3/4} T_f^{3/16} p_v^{-3/8} \tag{D16}$$

This expression contains only assigned parameters except for the tangential force coefficient C_F and p_v. As discussed earlier, we shall neglect changes in C_F due to changes in computed quantities; C_F is included to indicate the effect of possible errors in the assigned parameters that affect its value such as the constant C in equation (C3). The symbol p_v has been used here in place of 10^{c_1}, which appears in the equilibrium vapor pressure law (eq. (C11)) and is hence an assigned parameter. Substituting equation (D12) into (D16) leads to equation (17) of the text.

Additional approximate analyses and machine calculations have been made to determine the effects of changes in the parameters c_2 and i appearing in the viscosity and vapor pressure laws. Such variations were found to be approximately equivalent to changes in the parameters C_μ and p_v considered above except for an additional constant shift in the stagnation-point temperature. Machine calculations were also made with different values of the parameters appearing in equations (C2) through (C9), such as ϵ, ζ_v, and C_{ms}. For changes by as much as a factor of 2, the effects on m and τ_{op} were less than 30 percent as anticipated in the discussion preceding equation (D13).

Results from the approximations of this appendix are compared with results from machine calculations in the Results and Discussion section. The comparisons show that the approximations are reasonably accurate in the prediction of the effects of reassignment of all parameters except the froth density ρ_{mf}. Considerable insight into the problem under investigation is thereby afforded by the approximations as summarized in equations (16) and (17) of the text. How reassigning parameters affects computed quantities, such as mass, mean meteoroid density, or stagnation-point surface temperature, can be deduced from formulas contained in this appendix.

APPENDIX E

INTENSITY LAG EFFECT

Relationship Between τ_{opc} and τ_{op}

Equation (19) can be rewritten in terms of the known quantities

$$m_1(t) = \frac{2}{\tau_{op1}} \int_t^\infty \frac{I_p}{V^3} \, dt \tag{E1}$$

where τ_{op1} is the assumed constant value of luminous efficiency factor upon which the values of mass m_1 published in reference 5 are based. With the assumption that τ_{opc} is constant along the trajectory and upon substitution of equation (E1), equation (19) can be written

$$m(t) = \frac{\tau_{op1}}{\tau_{opc}} \{ m_1(t) + B[m_1(t + \theta) - m_1(t)] \} \tag{E2}$$

For small θ, $m_1(t + \theta)$ can be approximated by

$$m_1(t + \theta) = m_1(t) + \theta \dot{m}_1(t) \tag{E3}$$

and substituting this into equation (E2) yields

$$m(t) = \frac{\tau_{op1}}{\tau_{opc}} m_1(t) \left(1 + B\theta \frac{\dot{m}_1}{m_1} \right) \tag{E4}$$

Differentiating and combining equations (18) and (E1) leads to the relation

$$\dot{m}_1 = \frac{\tau_{op}}{\tau_{op1}} \dot{m} \tag{E5}$$

If τ_{op} in equation (18) is taken to be approximately constant along a trajectory so that τ_{op} can be taken outside the integral, combining the result with equation (E1) yields

$$m_1 = \frac{\tau_{op}}{\tau_{op1}} m \tag{E6}$$

Substituting equations (E5) and (E6) into (E4) leads to the approximate relation

$$\tau_{opc} = \tau_{op} \left(1 + B\theta \frac{\dot{m}}{m} \right)$$

which is equation (20) of the text.

Lag Time

An equation for the rate of ablation of froth particles in the wake can be written

$$\frac{1}{m_f} \frac{dm_f}{dt} = - \frac{1}{2} \frac{C_H \rho V^3}{\zeta} \frac{A_f}{m_f} \qquad (E7)$$

Substituting equations (4) and (5) leads to

$$m_f^{-2/3} \frac{dm_f}{dt} = -K_f \qquad (E8)$$

where

$$K_f = \frac{(1/2) C_H \rho V^3 S_F}{\zeta \rho_{mf}^{2/3}} \qquad (E9)$$

The integration of equation (E8) with K_f considered constant yields

$$m_{fo}^{1/3} - m_f^{1/3} = \frac{1}{3} K_f (t - t_o) \qquad (E10)$$

This relation indicates that the froth particle would ablate to nothing in a time

$$\theta = \frac{3 m_{fo}^{1/3}}{K_f} \qquad (E11)$$

Substituting equation (E9) yields

$$\theta = \frac{6 \zeta \rho_{mf}^{2/3} m_{fo}^{1/3}}{C_H \rho V^3 S_F}$$

which is equation (21) of the text.

According to reference 3, chapter 6, under air pressure, liquefied meteoric material will break up into drops of radius

$$r_l = 4.8 \frac{\tau_s}{\rho V^2} \qquad (E12)$$

where τ_s is the surface tension. In reference 15, the numerical value 2.6 is used in place of 4.8 in the above expression to indicate incipient disruption of a tektite drop. A value of the surface tension

$$\tau_s = 0.36 \text{ kg/sec}^2$$

is used for stone or pumice in reference 24. Ablation can occur only by vaporization for drops of the above size or smaller. Therefore, the specific heat of ablation ζ in equation (21) should be taken equal to ζ_v for such drops.

61

Substituting

$$m_l = \frac{4}{3} \pi \rho_{mf} r_l^3$$

and the shape factor for a sphere

$$S_F = \left(\frac{3}{4}\right)^{2/3} \pi^{1/3}$$

into equation (21) leads to

$$\theta_l = \frac{38.4 \zeta_v \rho_{mf} \tau_s V}{C_H (\rho V^3)^2} \tag{E13}$$

Evaluating this with $\zeta_v = 8.51 \times 10^6$, $\rho_{mf} = 100$ kg/m^3, $\tau_s = 0.36$ kg/sec^2, $V = 2 \times 10^4$ m/sec, $C_H = 1$ yields

$$\theta_l = 0.0235 \times (10^8/\rho V^3)^2$$

which is equation (25) of the text.

At an early part of the trajectory of meteor 4464 of reference 5 the impact pressure and velocity were

$$\rho V^2 = 3400 \text{ N/m}^2$$

$$V = 2 \times 10^4 \text{ m/sec}$$

Under these conditions and with the above value of surface tension, equation (E12) indicates

$$r_l = 5.1 \times 10^{-4} \text{ meter}$$

The corresponding values of mass m_l and θ_l are indicated in the text.

For solidified froth particles, an estimate of the initial mass m_{fo} is needed to determine θ_f from equation (21). The faintest meteors described in reference 20 show fluctuations in the light curves at a rate of about 15 fluctuations per second. According to the method of this report, meteor 4464 loses mass at about the rate of 4.5×10^{-4} kg/sec. If all the ablation is attributed to sloughing of froth particles, the mass per particle would be about

$$m_{fo} = 3 \times 10^{-5} \text{ kg}$$

Evaluation of equation (21) with $m_{fo} = 3 \times 10^{-5}$ kg and $\zeta = \zeta_v$ yields

$$\theta = 0.42 \text{ sec} \quad \text{(vaporization dominant)}$$

which is somewhat high compared to the value of the product $B\theta = 0.2$ second obtained for meteor 4464. Use of the viscous flow equations derived in appendix B leads to the conclusion that, for particles of the size and composition under consideration, ablation will occur largely by liquid run off rather than by evaporation. In that case the specific heat of ablation ζ in

equation (21) would be closer in value to ζ_f than ζ_v. The resulting computed lag time is

$$\theta_f = 0.092 \text{ sec} \quad \text{(liquid ablation dominant)}$$

Fragmentation of the froth particles may also play a role in producing a higher rate of vaporization of the particles in the wake than that occurring directly from the parent meteoroid.

The dependence of θ_f on ρV^3 is found by substituting $\zeta = 1.884 \times 10^6$, $\rho_{mf} = 100 \text{ kg/m}^3$, $m_{fo} = 3 \times 10^{-5}$ kg, $C_H = 1$, $S_F = (9\pi/16)^{1/3}$ in equation (21) to obtain

$$\theta_f = 0.063 \times 10^8 / \rho V^3$$

which is equation (24) of the text.

Lag Distance

A dynamic equation for the froth particles similar to equation (2) can be written

$$\dot{V}_f = -\frac{1}{2} C_D \rho V^2 \frac{A_f}{m_f}$$

Since the combination $C_D A/m_f$ is larger for the froth particles than for the parent meteoroid, they would be expected to lag behind once they were free of the protection of the stream in the immediate wake. According to W. A. Page of Ames Research Center, thin plastic disks have been observed to overtake and bump models of smaller $C_D A/m$ in free-flight tests. Thus it is possible that during deceleration an accumulation of froth builds up behind the parent meteoroid. However, we assume that froth particles can also escape into unprotected regions of the wake due to bumping or other dispersive influences. In that case, they will accelerate away from the parent meteoroid approximately at the rate

$$\Delta\dot{V}_f = \frac{1}{2} C_D \rho V^2 \frac{A_f}{m_f} \tag{E14}$$

If $\Delta\dot{V}_f$ is taken to be constant, the separation distance is

$$\Delta L = \frac{1}{2} \Delta\dot{V}_f (t - t_o)^2$$

and at a time $t - t_o = \theta$ will amount to

$$\Delta L = \frac{1}{2} \Delta\dot{V}_f \theta^2$$

Substituting the above expression for $\Delta\dot{V}_f$ and using equation (E9) to remove ρV^2 leads to

$$\Delta L = \frac{1}{2} \frac{K_f \theta}{m_{fo}^{1/3}} \frac{C_D \zeta \theta}{C_H V}$$

63

Substituting equation (E11) to remove K_f yields

$$\Delta L = \frac{3}{2} \frac{C_D \zeta \theta}{C_H V}$$

which is equation (22) of the text. An expression for ΔL with a numerical factor of 3 rather than 3/2 can be derived by considering the variability of A_f/m_f in equation (E14) rather than setting it equal to $S_F/(\rho_{mf}^{2/3} m_{fo}^{1/3})$. However, this value would be reduced if the smaller values of ρV^2 at the early part of the ablation process were taken into account. Therefore, we have used the above numerical value of 3/2 for estimating the lag distance.

REFERENCES

1. Jacchia, L. G.: The Physical Theory of Meteors. VIII. Fragmentation as Cause of the Faint-Meteor Anomaly. Astrophys. J., Vol. 121, no. 2, March 1955, pp. 521-527.

2. Whipple, F. L.: On Meteor Masses and Densities. Astron. J., vol. 58, 1952, pp. 28-29.

3. Öpik, Ernst J.: Physics of Meteor Flight in the Atmosphere. Interscience Publishers, Inc., 1958.

4. Allen, H. Julian; and Baldwin, Barrett S.: Frothing as an Explanation of the Acceleration Anomalies of Cometary Meteors. J. Geophys. Res., vol. 72, no. 13, July 1967, pp. 3483-3496.

5. Jacchia, Luigi G.; Verniani, Franco; and Briggs, Robert E.: An Analysis of the Atmospheric Trajectories of 413 Precisely Reduced Photographic Meteors. Smithsonian Inst. Ast. Obs. Research in Space Science Special Rept. 175, April 1965.

6. Verniani, Franco: On the Luminous Efficiency of Meteors. Smithsonian Contrib. Astrophys., vol. 8, no. 5, 1965, pp. 141-172.

7. Allen, H. Julian; and James, Nataline A.: Prospects for Obtaining Aerodynamic Heating Results From Analysis of Meteor Flight Data. NASA TN D-2069, 1964.

8. Cook, A. F.; Jacchia, L. G.; and McCrosky, R. E.: Luminous Efficiency of Iron and Stone Asteroidal Meteors. Smithsonian Contrib. Astrophys., vol. 7, 1963, pp. 209-220.

9. Whipple, Fred L.; and Jacchia, Luigi G.: Reduction Methods for Photographic Meteor Trails. Smithsonian Contrib. Astrophys., vol. 1, no. 2, 1957, pp. 183-206.

10. Posen, Annette; and McCrosky, Richard E.: A Theoretical Study of Meteoric Trajectories and Processes, Including Examination of the Incidence and Characteristics of Photographic Meteors by Reduction of About 600 Data Points. NASA CR-862, 1967.

11. Anon.: U. S. Standard Atmosphere 1962. Prepared under sponsorship of NASA, USAF, and USWB.

12. Matting, Fred W.; and Chapman, Dean R.: Analysis of Surface Ablation of Noncharring Materials With Description of Associated Computing Program. NASA TN D-3758, 1966.

13. Verniani, F.: On the Density of Meteoroids. II.- The Density of Faint Photographic Meteors. Il Nuovo Cimento. Serie X, vol. 33, no. 4, August 16, 1964, pp. 1173-1184.

14. Shepard, Charles E.; Vorreiter, John W.; Stine, Howard A.; and Winovich, Warren: A Study of Artificial Meteors as Ablators. NASA TN D-3740, 1967.

15. Chapman, Dean R.; and Larson, Howard K.: On the Lunar Origin of Tektites. J. Geophys. Res., vol. 68, no. 14, July 15, 1963, pp. 4305-4358.

16. Davis, J.; and Hall, J. E.: Meteor Luminosity and Ionization. Proc. Roy. Soc. (London), Ser. A, vol. 271, no. 344, Jan. 1, 1963, pp. 120-128.

17. Ayers, Wendell G.: Luminous Efficiency of an Artificial Meteor at 11.9 Kilometers per Second. NASA TN D-2931, 1965.

18. Friichtenicht, J. C.; Slattery, J. C.; and Tagliaferri, E.: A Laboratory Measurement of Meteor Luminous Efficiency. NASA CR-787, 1967.

19. Jacchia, Luigi G.; and Whipple, Fred L.: Precision Orbits of 413 Photographic Meteors. Smithsonian Contrib. Astrophys., vol. 4, no. 4, 1961.

20. Ceplecha, Z.; and Jezkova, M.: Detailed Data on Ondrejov Double-Station Meteors During IGY and IGC. Astronomical Institute of Czechoslovakia Bulletin, vol. 16, no. 3, 1965, pp. 166-189.

21. Landolt, Hans H.; and Börnstein, Richard, eds.: Zahlenwerte und Funktionen aus Physik, Chemie, Astronomie, Geophysik, und Technik. IV Band, 1 Teil Staffwerte und Mechanisches Verhalten von Nichtmetallen, 1955, pp. 585-661.

22. Centolanzi, Frank J.; and Chapman, Dean R.: Vapor Pressure of Tektite Glass and Its Bearing on Tektite Trajectories Determined From Aerodynamic Analysis. J. Geophys. Res., vol. 71, no. 6, March 15, 1966, pp. 1735-1749.

23. Joos, Georg: Theoretical Physics. Third ed., Hafner Publishing Co., New York, 1958.

24. Allen, H. Julian; Baldwin, Barrett S.; and James, Nataline A.: Effect on Meteor Flight of Cooling by Radiation and Ablation. NASA TN D-2872, 1965.

TABLE I.- ASSUMED VALUES OF CONSTANTS AND PARAMETERS[a]

Quantity	Value, MKS	Name
A_{rn}	1.0	Shape parameter
A_{rs}	0.874	Shape parameter
C	0.943×10^{-4}	Heat-transfer parameter
C_1	10.63	Parameter in vapor pressure law
C_2	-16,750	Parameter in vapor pressure law
C_{ms}	0.15	Parameter in energy equation
C_μ	1.525×10^{-8}	Parameter in viscosity law
i	14,800	Parameter in viscosity law
k	2.0	Thermal conductivity
M	0.03985	Molecular weight
P_v	0.15	Heat-transfer parameter
S_F	1.919	Shape factor
T_f	1785	Fusion temperature
α	0.3	Heat-transfer parameter
ϵ	0.6	Radiative emissivity
ρ_{21}	9	Density ratio for normal shock
ρ_{mf}	100	Froth density
ρ_{ms}	2,800	Solid density
σ_1	0.1	Heat-transfer parameter
ζ_f	1.884×10^6	Specific heat of fusion
ζ_v	8.51×10^6	Specific heat of vaporization

[a]Material properties correspond to carbonaceous chondrite.

TABLE II.- TRAIL NUMBERS IN 40-METEOR SAMPLE

3,076[a]	4,464[a]	6,949[a]	7,161[a]	7,216[a]	7,272[a]
8,447	8,469	8,726	8,766[a]	8,881[a]	8,891
8,945	8,990	9,015[a]	9,030	9,170	9,416[a]
9,880	9,888[a]	9,900	9,917	10,070[a]	10,094
10,240	10,358	10,384[a]	10,414[a]	10,439	10,447
11,825	11,856	11,973	12,342	12,361	12,363
12,399	12,504[a]	12,577	12,714		

[a]Meteors for which intensity lag times and corrected values of luminous efficiency factor were computed.

"The aeronautical and space activities of the United States shall be conducted so as to contribute . . . to the expansion of human knowledge of phenomena in the atmosphere and space. The Administration shall provide for the widest practicable and appropriate dissemination of information concerning its activities and the results thereof."

— NATIONAL AERONAUTICS AND SPACE ACT OF 1958

NASA SCIENTIFIC AND TECHNICAL PUBLICATIONS

TECHNICAL REPORTS: Scientific and technical information considered important, complete, and a lasting contribution to existing knowledge.

TECHNICAL NOTES: Information less broad in scope but nevertheless of importance as a contribution to existing knowledge.

TECHNICAL MEMORANDUMS: Information receiving limited distribution because of preliminary data, security classification, or other reasons.

CONTRACTOR REPORTS: Scientific and technical information generated under a NASA contract or grant and considered an important contribution to existing knowledge.

TECHNICAL TRANSLATIONS: Information published in a foreign language considered to merit NASA distribution in English.

SPECIAL PUBLICATIONS: Information derived from or of value to NASA activities. Publications include conference proceedings, monographs, data compilations, handbooks, sourcebooks, and special bibliographies.

TECHNOLOGY UTILIZATION PUBLICATIONS: Information on technology used by NASA that may be of particular interest in commercial and other non-aerospace applications. Publications include Tech Briefs, Technology Utilization Reports and Notes, and Technology Surveys.

Details on the availability of these publications may be obtained from:

SCIENTIFIC AND TECHNICAL INFORMATION DIVISION

NATIONAL AERONAUTICS AND SPACE ADMINISTRATION
Washington, D.C. 20546